Received 22 September 2025; revised 25 November 2025; accepted 9 December 2025. Date of publication 15 December 2025; date of current version 24 December 2025.

Digital Object Identifier 10.1109/OJCOMS.2025.3644171

Cell-Free Macro-Diversity Schemes in LEO Non-Terrestrial Networks With OTFS and OFDM Modulations

CARMEN D'ANDREA [1,2,3] (Member, IEEE), TOMMASO FOGGI [3,4] (Member, IEEE), AMINA PIEMONTESE [3,4] (Member, IEEE), ALESSANDRO UGOLINI [3,4] (Member, IEEE), STEFANO BUZZI [1,2,3,5] (Senior Member, IEEE), AND GIULIO COLAVOLPE [3,4] (Senior Member, IEEE)

[1]Dipartimento di Ingegneria Elettrica e dell'Informazione, University of Cassino and Southern Lazio, 03043 Cassino, Italy
[2]European University of Technology EUt+, Cassino, European Union
[3]Consorzio Nazionale Interuniversitario per le Telecomunicazioni, 43124 Parma, Italy
[4]Dipartimento di Ingegneria e Architettura, University of Parma, 43124 Parma, Italy
[5]Dipartimento di Elettronica, Informazione e Bioingegneria, Politecnico di Milano, 20122 Milan, Italy

CORRESPONDING AUTHOR: C. D'ANDREA (e-mail: carmen.dandrea@unicas.it)

This work was supported in part by the European Union under the Italian National Recovery and Resilience Plan (NRRP) of NextGenerationEU; in part by the Partnership on "Telecommunications of the Future" (PE00000001—Program "RESTART," Structural Project ITA NTN, Cascade Call INFINITE and Structural Project 6GWINET, Cascade Call SPARKS); in part by the PRIN 2022 Project titled "INSPIRE: Integrated Terrestrial/Space Wireless Networks for Broadband Connectivity and IoT Services" funded by the Italian Ministry of Universities and Research (MUR) under Grant 2022BEXMXN_01; and in part by the European Union Smart Networks and Services Joint Undertaking Project 5G-STARDUST under Grant 101096573.

ABSTRACT Satellite-based Non-Terrestrial Networks, particularly those using large constellations of Low Earth Orbit (LEO) satellites, are expected to play a critical role in enabling global 6G connectivity. While offering promising coverage and capacity, LEO systems face challenges such as intermittent link blockages and high Doppler shifts, especially in mobile or obstructed environments. To mitigate these issues, this paper investigates advanced macro-diversity techniques tailored for LEO satellite systems. Inspired by user-centric cell-free massive MIMO architectures in terrestrial networks, we propose a comprehensive end-to-end transceiver model that captures the complete signal chain, from symbol generation and continuous-time waveform transmission to receiver-side sampling and data detection. Crucially, we account for satellite-specific Doppler shifts and phase offsets, often overlooked in simplified models. We analyze and compare two modulation schemes: traditional OFDM and OTFS, the latter offering enhanced resilience to time-varying channels. Furthermore, we consider the case of multi-antenna user terminals (UTs) and demonstrate how receive beamforming can effectively mitigate inter-satellite phase misalignment, significantly improving system robustness and performance. The obtained numerical results show the effectiveness of the proposed schemes, confirm the superiority of the OTFS modulation w.r.t. OFDM, and provide evidence that multiple antennas at the UT can be exploited to overcome the phase misalignment effects of downlink signals coming from different serving LEO satellites. Finally, results also show that satellite-UT association schemes may have a considerable impact on system performance.

INDEX TERMS LEO satellites, non-terrestrial network (NTN), cell-free massive MIMO, user-centric, OFDM, OTFS.

I. INTRODUCTION

NON-TERRESTRIAL networks (NTNs) are expected to play a key role in the development of future 6G wireless communications by facilitating universal and global connectivity, especially in remote, underserved, or infrastructure-deficient areas [1], [2]. Indeed, one of the most disruptive features of 6G is to achieve ubiquitous and fair connectivity, and it is generally recognized that terrestrial cellular coverage alone cannot be able to overcome the "digital divide" [3], [4]. Furthermore, NTNs become

critically important in high-demand traffic conditions, as they can relieve the load on land-based networks, or in emergency or disaster situations where terrestrial infrastructures may be compromised. Reflecting their strategic importance, NTNs are attracting increasing attention within the 6G research and development community, and standardization efforts are actively progressing in this area [5], [6]. Broadly, the term NTN encompasses a diverse set of platforms, including Unmanned Aerial Vehicles (UAVs), high-altitude platform stations (HAPS), and satellites in various orbital regimes.

In recent years, a surge of interest has emerged around satellite-based NTNs, particularly mega-constellations composed of thousands of small satellites deployed in low-earth orbit (LEO). Given the benefits of ubiquitous coverage, among others immunity to disasters and low deployment complexity, the LEO megaconstellations, SpaceX's Starlink stands out as one of the most prominent and operationally advanced examples, are being considered as a complementary design for global coverage, playing essential roles in 6G [7], [8], [9].

Despite very good performance levels, it should be noted that LEO-based connectivity also introduces unique challenges. Specifically, when considering mobile user terminals (UTs), a line-of-sight (LOS) link between the LEO satellite and the terrestrial UT is not always granted: due to the fast movement of the satellite, the LOS link can be indeed unexpectedly shadowed/obstructed by physical objects nearby the UT. Satellite macro-diversity schemes, i.e., the joint use of several satellites to serve the same UT, can be widely used in order to increase the system reliability and efficiency [10], [11], [12], [13]. The results of these papers show that, under the assumption that the satellites serving the same UT are widely separated in the angle domain, the blockage events for each UT-satellite link are statistically independent, which leads to an exponential decrease of the probability that a UT is completely blocked on all of its active links.

Building on our earlier work [10], [11], [14], this paper investigates macro-diversity strategies for LEO satellite systems. These strategies are inspired by the architectural principles and rich body of research developed for user-centric cell-free (UC-CF) massive multiple-input multiple-output (MIMO) systems in terrestrial networks [15], [16]. In contrast to the aforementioned studies, we explicitly address the challenge that information signals arriving at the UT from different satellites may be subject to distinct Doppler shifts and phase offsets. Furthermore, while much of the related literature adopts simplified single-frequency discrete-time signal models, we instead provide a comprehensive end-to-end transceiver model. This model encompasses the entire signal processing chain–from the generation of information symbols and their mapping into continuous-time waveforms, through transmission over the air interface, to signal sampling at the receiver and subsequent data detection. In doing so, we consider two modulation schemes: the conventional orthogonal frequency division multiplexing (OFDM), and the more recent orthogonal time frequency space (OTFS), which has been advocated for its robustness in highly time-varying channels, such as those encountered in LEO satellite scenarios. Furthermore, the relevant case that the UT is equipped with multiple antennas is considered, and the paper also shows how receive beamforming can be used to cope with the problem of the phase misalignment in the signal components arriving from different satellites.

A. RELATED WORKS

The structural similarities between LEO satellite mega-constellations and UC-CF massive MIMO terrestrial systems, relying on dense access points (APs) deployments, have sparked growing interest in the adaptation of UC-CF inspired macro-diversity strategies to NTNs. In terrestrial UC-CF networks, coherent processing is widely adopted: APs estimate the uplink channel through training sequences transmitted on the uplink and, under the assumption of time division duplexing (TDD), exploit channel reciprocity for downlink beamforming and uplink combining [15], [16], [17], [18]. While most of the literature on terrestrial UC-CF massive MIMO assumes perfect phase alignment among the signals transmitted to the same user from different APs, more recently non-coherent approaches have emerged. For instance, the paper [19] proposes a diversity-based scheme using Alamouti-like space-time coding to combat deep fades without requiring phase coherence, while [20] addresses these problems through the use of differential techniques.

When applying UC-CF massive MIMO concepts to LEO NTNs, challenging specificities emerge. Indeed, in the NTNs scenario uplink channel estimation and phase compensation are extremely challenging due to satellite mobility and propagation delays [10], [11]. While Doppler and timing compensation can be accurately performed at known ground locations, phase alignment across multiple satellites is generally impractical. Thus, simply transplanting terrestrial UC-CF designs to satellite-based NTNs is not straightforward, necessitating novel solutions to fully leverage macro-diversity. These limits are explored in [14], by comparing coherent and non-coherent joint transmissions and highlighting the need for at least coarse phase alignment to approach satisfactory performance.

The literature on UC-CF NTNs is rapidly expanding, with diverse directions explored. In [21], a non-geosynchronous satellite system is considered, and a location-based minimum-mean-squares error (MMSE) beamforming strategy is proposed to address channel state information (CSI) uncertainty. The formation-of-arrays (FoA) concept, introduced in [22], [23], envisions distributed antenna arrays formed by small satellites flying in coordinated clusters. These studies investigate system-level issues such as geometry, synchronization, and radio resource management, drawing direct parallels with UC-CF networks. Hybrid terrestrial-satellite architectures have also been considered.

In [24], the authors propose offloading users from a UC-CF terrestrial segment to a LEO-based segment to balance load and improve scalability. In [25], a cognitive satellite-UAV network is proposed, where UAV swarms provide on-demand cell-free coverage. A terrestrial cell-free massive MIMO network supported by a LEO satellite is analyzed in [26], assuming uplink channel estimation and optimizing scheduling and transmit power for throughput maximization. Focusing on physical-layer techniques, [27] proposes a coordinated multi-satellite OTFS transmission strategy, using an aggregate channel estimation scheme that jointly estimates all satellite-to-ground links as a single equivalent channel. Advanced signal processing and artificial intelligence (AI) techniques have also been explored. A notable example is presented in [28], where a lightweight AI model is proposed to predict channel statistics, such as line-of-sight (LOS) blockage correlations, thereby refining CSI feedback and improving system performance. The proposed approach achieves up to a 15% capacity gain and reduced outage rates. In [29], statistical CSI is used to dynamically form satellite clusters and coordinate their transmission, reducing handover rates and interference, with improved spectral efficiency and coverage. While [28] and [29] address UC-CF NTN scenarios similar to ours, they focus primarily on high-level resource optimization and CSI prediction, neglecting core physical-layer challenges, such as designing beamforming strategies in the absence of phase knowledge and evaluating performance under realistic multi-carrier transmission assumptions. Finally, [30] examines a satellite-UAV UC-CF network, where UAVs act as APs to extend satellite coverage. A successive convex approximation algorithm for maximizing downlink energy efficiency under UAV power and QoS constraints is thus proposed.

B. PRACTICAL ASPECTS

In this paper, ideal channel estimation, i.e., perfect channel state information at the receiver, is assumed, since the aim of the proposed system architecture and the analysis of its performance is the demonstration of the feasibility of the UC-CF approach for satellite communications rather than the investigation of the impact of realistic estimation strategies over OTFS and OFDM systems, a topic which is widespread in literature. Also, the reader can refer to [31] for an in-depth analysis, including the detection complexity comparison, carried out by some of the same authors. Basically, the presence of pilots would entail an overhead on the detector performance whose impact can be easily derived, whereas an imperfect estimation of channel coefficients, Doppler shifts, and delays would imply a penalty that depends on the chosen algorithm, channel realization, and parameter configuration. Such analysis falls outside the scope of this paper, but represents a relevant topic for future investigations.

Moreover, the beamforming design here proposed only relies on the relative position of transmitter and receiver, which can be considered basically constant over time spans orders of magnitude larger than the duration of transmitted data frames, therefore any processing on both sides would be critical only from the precision (i.e., positioning error) point of view rather than for the computational load. In any case, it does not depend on the modulation format. As far as the detection processing complexity is concerned, the reader is referred to [32], [33]. Also consider that any complexity-related aspects involved in the detection and beamforming processing at both transmit and receive ends strongly depend on the computational capabilities that will be enabled in the next years, whose analysis falls outside the scope of this work.

Another key practical consideration is the mitigation of phase misalignments to preserve signal integrity between satellites and UTs. This challenge, inherent to UC-CF massive MIMO systems [20], [34], can be addressed through per-satellite synchronization schemes such as the one proposed in [35], which employs space–time block coding and enables independent synchronization to handle unsynchronized transmissions while reducing UT RF complexity.

The impact of hardware impairments in the design of communication systems, which affect both terrestrial and non-terrestrial UC-CF massive MIMO architectures is another practical aspect that deserves to be considered. Relevant studies addressing this issue include [36], [37], [38].

Finally, radio resource management (RRM) and user scheduling are important considerations in satellite communications and remain significant research challenges in the scenario addressed in this paper. Although these aspects are beyond the scope of the present work, extensive literature on the topic is available, including [13], [39], [40], [41].

C. PAPER CONTRIBUTION

The main idea of this paper is to take advantage of a LEO mega-constellation to offer a more reliable and stable connection to the served UTs, mimicking a terrestrial UC-CF massive MIMO approach, taking into account the peculiarities of the satellite channel which are intrinsically different from the terrestrial one. It builds upon our earlier works [10], [11], [14], where preliminary studies on this topic have been reported. In particular, in [10], [11] the benefits of LEO satellite macro-diversity schemes have been described considering a more simple scenario compared to this paper (single user with single antenna) and the advantages of OTFS modulation with respect to the classical OFDM modulation have been discussed. In [14] preliminary studies on the framework here considered, i.e., the multi user scenario, have been reported assuming single-antenna receivers and OFDM modulation only, discussing the impact of phase misalignments of different signal contributions at the receiver. To the best of our knowledge, this is the first paper which rigorously addresses the use of satellite macro-diversity schemes in multiuser scenarios with both OFDM and OTFS waveforms and with explicit consideration of phase misalignments and Doppler shifts; moreover, in our scenario, the presence of multiple antennas at the UTs is

accounted for and exploited to solve the phase ambiguity problems on the downlink. Specifically, with respect to the current literature, the contribution of this paper can be summarized as follows.

- We propose a detailed transceiver model that captures the complete physical-layer processing in LEO satellite networks by considering the conventional OFDM and the more recent OTFS modulations, moving beyond simplified discrete-time models commonly used in the literature, and focusing on time-continuous waveforms.
- We focus on the case of multi-antenna UTs and propose to exploit receive beamforming to mitigate the phase misalignment between signals transmitted by different satellites, thereby providing a practical and easily implementable solution capable of improving link robustness and system performance.
- We propose beamforming schemes that can be implemented based on an (even approximate) knowledge of the UT position, with no need for accurate CSI as happens in terrestrial UC-CF massive MIMO networks.
- Heuristic association schemes between satellites and UTs are proposed and analyzed, also taking into account the fact that close UTs should not be served by the same satellite in the same time-frequency resource slot.
- A thorough and comprehensive numerical evaluation of the proposed schemes is performed in terms of achieved downlink signal-to-interference-plus-noise ratio (SINR) at the UT and pragmatic capacity.

Overall, the obtained results confirm that OTFS, despite higher complexity, generally outperforms the OFDM modulation. Moreover, results show that UTs having a single antenna enjoy limited macro-diversity benefits due to signal phase misalignments, but equipping UTs with multiple antennas and using proper beamforming schemes enables effective signal separation and significantly improves SINR and reliability. Furthermore, results show that satellite-UT association strategies that cap the number of served UTs or enforce angular separation improve SINR by reducing interference. Finally, pragmatic capacity results confirm that the maximum number of served UTs per satellite significantly impacts receiver performance, while the minimum angular distance constraint has a comparatively smaller influence.

D. PAPER ORGANIZATION

This paper is organized as follows. The next section introduces the considered system model and outlines the signal model for both the OFDM and the OTFS modulations. Section III deals with the description of the receiver processing that is needed at the UT to recover the information symbols, while in Section IV further aspects of the system design, such as the choice of the satellite and UT beamformers, of the power control strategy, and of the satellite–UT association strategy, are discussed. Section V is devoted to the description of the considered performance measures and to the discussion of the numerical results, while, finally, concluding remarks are given in Section VI.

E. NOTATION

We use non-bold letters for scalars, a and A, lowercase boldface letters, $\mathbf{a}$, for vectors and uppercase boldface letters, $\mathbf{A}$, for matrices. The transpose, the inverse and the conjugate transpose of a matrix $\mathbf{A}$ are denoted by $\mathbf{A}^T$, $\mathbf{A}^{-1}$ and $\mathbf{A}^H$, respectively. The (ℓ, m)-th entry, the ℓ-th row and the m-th column of the matrix $\mathbf{A}$ are denoted by $\mathbf{A}(\ell, m)$, $\mathbf{A}(\ell, :)$, $\mathbf{A}(:, m)$, respectively. The trace and the main diagonal of the matrix $\mathbf{A}$ are denoted as $\mathrm{tr}(\mathbf{A})$ and $\mathrm{diag}(\mathbf{A})$, respectively. The diagonal matrix obtained from the vector $\mathbf{a}$ is denoted by $\mathrm{diag}(\mathbf{a})$. The block-diagonal matrix obtained from matrices $\mathbf{A}_1, \ldots, \mathbf{A}_N$ is denoted by $\mathrm{blkdiag}(\mathbf{A}_1, \ldots, \mathbf{A}_N)$. The operator that returns an orthonormal basis for the range of $\mathbf{A}$ is denoted by $\mathrm{orth}(\mathbf{A})$. The N-dimensional identity matrix is denoted as $\mathbf{I}_N$, the $(N \times M)$-dimensional matrix with all zero entries is denoted as $\mathbf{0}_{N\times M}$ and $\mathbf{1}_{N\times M}$ denotes a $(N \times M)$-dimensional matrix with unit entries. The statistical expectation and variance operators are denoted as $\mathbb{E}[\cdot]$ and $\mathrm{var}\{\cdot\}$ respectively; $\mathcal{CN}(\mu, \sigma^2)$ denotes a complex circularly symmetric Gaussian random variable with mean μ and variance σ^2.

II. SYSTEM AND SIGNAL MODELS

We now outline the system and signal models considered in this paper. We consider a terrestrial area containing Q UTs equipped with uniform planar arrays (UPAs) with N_{UT} antennas. For the sake of simplicity, all UTs are assumed to have the same number of antennas. The Q UTs are in possible visibility with P satellites, all equipped with UPAs having the same number N_{S} of antennas. The representation of the considered scenario is reported in Figure 1, where we see that some paths from satellites to UTs can be blocked by the presence of obstacles. We denote by M the number of subcarriers, Δ_f the subcarrier spacing, $W = \Delta_f M$ the system bandwidth, N the number of symbols, T is the symbol duration, and $T_{\mathrm{frame}} = NT$ the frame duration. We also assume $T\Delta_f = 1$.

A. CHANNEL MODEL

The downlink time-varying channel between the q-th UT and the p-th satellite is the following vector-valued $(N_{\mathrm{UT}} \times N_{\mathrm{S}})$-dimensional function:

$$\mathbf{H}_{p,q}(t,\tau) = \rho_{p,q}\mathbf{a}_{\mathrm{UT}}\left(\phi^{\mathrm{UT}}_{p,q}, \theta^{\mathrm{UT}}_{p,q}\right)\mathbf{a}^T_{\mathrm{S}}\left(\phi^{\mathrm{S}}_{p,q}, \theta^{\mathrm{S}}_{p,q}\right) \times \delta\left(\tau - \tau_{p,q}\right)e^{j2\pi\nu_{p,q}t}, \quad (1)$$

where

- $\rho_{p,q}$ is the *complex gain* containing the path-loss, log-normal shadowing loss and clutter loss, i.e., the attenuation due to surrounding objects on the ground,
- $\phi^{\mathrm{S}}_{p,q}$ and $\theta^{\mathrm{S}}_{p,q}$ are the azimuth and elevation angles corresponding to the direction of departure (DoD),

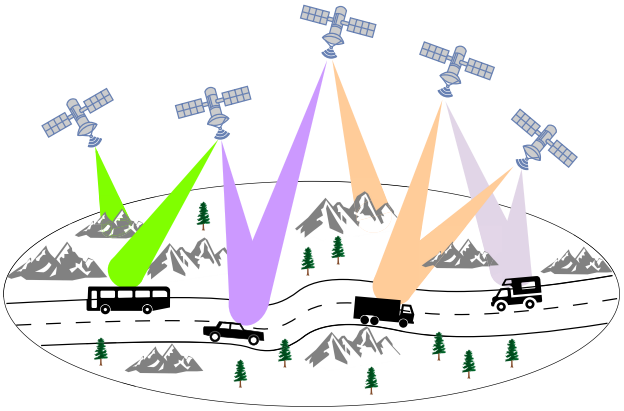

FIGURE 1. Schematic representation of the considered scenario, where each terrestrial UT is served by a personal cluster of LEO satellites. Some potential paths from satellites to UTs are blocked by obstacles.

- $\phi_{p,q}^{\mathrm{UT}}$ and $\theta_{p,q}^{\mathrm{UT}}$ are the azimuth and elevation angles corresponding to the direction of arrival (DoA),
- $\mathbf{a}_x(\varphi, \vartheta)$ is the UPA array response, specified later, at the generic array, i.e., $x \in \{\mathrm{S}, \mathrm{UT}\}$,
- $N_{\mathrm{S}} = N_{\mathrm{S,v}} N_{\mathrm{S,h}}$ is the number of antennas at the satellite with $N_{\mathrm{S,v}}$ and $N_{\mathrm{S,h}}$ the number of antennas on the vertical and horizontal axis, respectively,
- $N_{\mathrm{UT}} = N_{\mathrm{UT,v}} N_{\mathrm{UT,h}}$ is the number of antennas at the UT with $N_{\mathrm{UT,v}}$ and $N_{\mathrm{UT,h}}$ the number of antennas on the vertical and horizontal axis, respectively,
- $\tau_{p,q}$ and $\nu_{p,q}$ are the *residual* propagation delay and the Doppler shift of the q-th UT with respect to the p-th satellite.

Note that $\nu_{p,q}$ is a *relative Doppler shift* that takes into account the movement of the p-th satellite and the q-th UT. To mimicking the actual working conditions of the satellites systems, we assume that the satellites perfectly compensate for delay and Doppler shift in one specific location, namely, the *ideal UT position*. The delays and Doppler shifts, i.e., $\tau_{p,q}$ and $\nu_{p,q}$ in (1), are residual uncompensated values given by the location uncertainty, *offset distance* $r_{p,q}$ say, of the UT from the ideal position known at the satellite.[1]

Regarding the definition of the UPA array response, upon defining the wave vector $\mathbf{k}(\varphi, \vartheta)$ as

$$\mathbf{k}(\varphi, \vartheta) = \frac{2\pi}{\lambda}[\cos\vartheta\cos\varphi, \cos\vartheta\sin\varphi, \sin\vartheta]^T, \tag{2}$$

with λ the signal carrier wavelength, the array response is written as

$$\mathbf{a}_x^T(\varphi, \vartheta) = \sqrt{\Gamma_x}\left[e^{j\mathbf{k}^T(\varphi,\vartheta)\mathbf{u}_x(1)}, \ \ldots, \ e^{j\mathbf{k}^T(\varphi,\vartheta)\mathbf{u}_x(N_x)}\right], \tag{3}$$

where again $x \in \{\mathrm{S}, \mathrm{UT}\}$, $\mathbf{u}_x(n_x)$, $n_x = 1, \ldots, N_x$, is the position of the n_x-th antenna on the satellite and Γ_x is the gain of the generic radiation element [22].

[1]The entity of the offset distance must be properly designed considering the capability of the modulation format to estimated the given relative delays and Doppler shifts.

B. OTFS SIGNAL MODEL

We focus on a generic block of NM symbols and denote by $x_{k,\ell}^{(q)}$ the symbol intended for the q-th UT on the downlink in the delay-Doppler domain with $k = 0, \ldots, N-1$ and $\ell = 0, \ldots, M-1$ belonging to a QAM constellation. Each satellite serving the q-th UT applies the inverse symplectic fast Fourier transform (ISFFT) converting the delay-Doppler domain signal to the time-frequency domain signal $X_{n,m}^{(q)}$ where [31]

$$X_{n,m}^{(q)} = \sum_{k=0}^{N-1}\sum_{\ell=0}^{M-1} x_{k,\ell}^{(q)} e^{j2\pi\left(\frac{kn}{N} - \frac{\ell m}{M}\right)}, \tag{4}$$

with $n = 0, \ldots, N-1$ and $m = 0, \ldots, M-1$. The signal transmitted at the p-th satellite is the following N_{S}-dimensional continuous time function

$$\mathbf{s}_p(t) = \sum_{q=0}^{Q-1} \alpha_{p,q}\sqrt{\eta_{p,q}}\mathbf{w}_{p,q} \times \sum_{n=0}^{N-1}\sum_{m=0}^{M-1} X_{n,m}^{(q)} g_{TX}(t - nT) e^{j2\pi m\Delta_f(t-nT)}, \tag{5}$$

with $\alpha_{p,q}$ a binary variable being 1 if the p-th satellite serves the q-th UT and 0 otherwise, $\eta_{p,q}$ the power transmitted from the p-th satellite to the q-th UT, $\mathbf{w}_{p,q}$ the N_{S}-dimensional beamforming vector used at the p-th satellite to serve the q-th UT and $g_{TX}(\cdot)$ the transmit shaping pulse. Denoting by $\mathbf{v}_{p^*,q}$ the N_{UT}-dimensional receive beamforming, also known as *combining*, vector at the q-th UE used to detect the signal transmitted from the p^*-th satellite, the received signal is written as

$$r_{p^*,q}(t) = \sum_{p=0}^{P-1} \mathbf{v}_{p^*,q}^T \int \mathbf{H}_{p,q}(t,\tau)\mathbf{s}_p(t-\tau)d\tau + \mathbf{v}_{p^*,q}^T\mathbf{z}_q(t), \tag{6}$$

where $\mathbf{z}_q(t)$ denotes the additive white Gaussian noise. By using the expression of $\mathbf{H}_{p,q}(t,\tau)$ in (1), the signal received at the q-th UT can be written as

$$r_{p^*,q}(t) = \sum_{p=0}^{P-1} \rho_{p,q}\mathbf{v}_{p^*,q}^T\mathbf{a}_{\mathrm{UT}}\left(\phi_{p,q}^{\mathrm{UT}}, \theta_{p,q}^{\mathrm{UT}}\right) \times \mathbf{a}_{\mathrm{S}}^T\left(\phi_{p,q}^{\mathrm{S}}, \theta_{p,q}^{\mathrm{S}}\right)\mathbf{s}_p\left(t - \tau_{p,q}\right)e^{j2\pi\nu_{p,q}t} + \mathbf{v}_{p^*,q}^T\mathbf{z}_q(t). \tag{7}$$

Substituting the expression of $\mathbf{s}_p(t)$ in (5) and after some manipulations we obtain (8), shown at the bottom of the next page.

The output of the RX filter bank adopting a generic receive shaping pulse $g_{RX}(t)$ is given by

$$Y_{p^*,q}(t,f) = \int r_{p^*,q}(t')g_{RX}^*(t'-t)e^{-j2\pi ft'}\mathrm{d}t' = \sum_{p=0}^{P-1} \rho_{p,q}\mathbf{v}_{p^*,q}^T\mathbf{a}_{\mathrm{UT}}\left(\phi_{p,q}^{\mathrm{UT}}, \theta_{p,q}^{\mathrm{UT}}\right)\mathbf{a}_{\mathrm{S}}^T\left(\phi_{p,q}^{\mathrm{S}}, \theta_{p,q}^{\mathrm{S}}\right) \times \mathbf{w}_{p,q'}\sum_{q'=0}^{Q-1}\alpha_{p,q'}\sqrt{\eta_{p,q'}}\sum_{n'=0}^{N-1}\sum_{m'=0}^{M-1} X_{n',m'}^{(q')}$$

$$\times \int g_{TX}(t'-n'T-\tau_{p,q})g^*_{RX}(t'-t)$$
$$\times e^{j2\pi m'\Delta_f(t'-n'T-\tau_{p,q})}e^{j2\pi\nu_{p,q}t'}e^{-j2\pi ft'}\mathrm{d}t' + \mathbf{v}^T_{p^*,q}\bar{\mathbf{z}}_q(t,f) \quad (9)$$

where $\bar{\mathbf{z}}_q(t,f)$ is the filtered noise at the receiver.

By sampling at $t=nT$ and $f=m\Delta_f$ we obtain the signal

$$Y^{(p^*,q)}_{n,m} = Y_q(t,f)|^{f=m\Delta_f}_{t=nT} = \sum_{p=0}^{P-1}\rho_{p,q}\mathbf{v}^T_{p^*,q}\mathbf{a}_{\mathrm{UT}}\left(\phi^{\mathrm{UT}}_{p,q},\theta^{\mathrm{UT}}_{p,q}\right)$$
$$\times \mathbf{a}^T_{\mathrm{S}}\left(\phi^{\mathrm{S}}_{p,q},\theta^{\mathrm{S}}_{p,q}\right)\sum_{q'=0}^{Q-1}\alpha_{p,q'}\sqrt{\eta_{p,q'}}\mathbf{w}_{p,q'}\sum_{n'=0}^{N-1}\sum_{m'=0}^{M-1}X^{(q')}_{n',m'}$$
$$\times \int g_{TX}(t'-n'T-\tau_{p,q})g^*_{RX}(t'-nT)$$
$$\times e^{j2\pi m'\Delta_f(t'-n'T-\tau_{p,q})}e^{j2\pi\nu_{p,q}t'}e^{-j2\pi m\Delta_f t'}\mathrm{d}t' + Z^{(p^*,q)}_{n,m}, \quad (10)$$

with $Z^{(p^*,q)}_{n,m} = \mathbf{v}^T_{p^*,q}\overline{\mathbf{Z}}^{(q)}_{n,m}$, and $\overline{\mathbf{Z}}^{(q)}_{n,m}$ the sampled version of $\bar{\mathbf{z}}_q(t,f)$.

It can be shown that $Y^{(p^*,q)}_{n,m}$ can be written as

$$Y^{(p^*,q)}_{n,m} = \sum_{p=0}^{P-1}\widetilde{\rho}_{p,q}\mathbf{v}^T_{p^*,q}\mathbf{a}_{\mathrm{UT}}\left(\phi^{\mathrm{UT}}_{p,q},\theta^{\mathrm{UT}}_{p,q}\right)\mathbf{a}^T_{\mathrm{S}}\left(\phi^{\mathrm{S}}_{p,q},\theta^{\mathrm{S}}_{p,q}\right)$$
$$\times \sum_{q'=0}^{Q-1}\alpha_{p,q'}\sqrt{\eta_{p,q'}}\mathbf{w}_{p,q'}\sum_{n'=0}^{N-1}\sum_{m'=0}^{M-1}X^{(q')}_{n',m'}$$
$$\times C_{n,n',m,m'}(\tau_{p,q},\nu_{p,q}) + Z^{(p^*,q)}_{n,m}, \quad (11)$$

where $\widetilde{\rho}_{p,q} = \rho_{p,q}e^{j2\pi\nu_{p,q}\tau_{p,q}}$, and

$$C_{n,n',m,m'}(\tau_{p,q},\nu_{p,q}) = C_{g_{TX},g_{RX}}\big((n-n')T -$$
$$\tau_{p,q},(m-m')\Delta_f-\nu_{p,q}\big)e^{j2\pi\nu_{p,q}n'T}e^{-j2\pi m\Delta_f\tau_{p,q}}, \quad (12)$$

and where we defined the cross ambiguity function

$$C_{u,v}(\tau,\nu) = \int u(s)v^*(s-\tau)e^{-j2\pi\nu s}\mathrm{d}s. \quad (13)$$

Finally, at the receiver the symplectic fast Fourier transform (SFFT) is applied, yielding

$$y^{(p^*,q)}_{k,\ell} = \frac{1}{NM}\sum_{n=0}^{N-1}\sum_{m=0}^{M-1}Y^{(p^*,q)}_{n,m}e^{j2\pi\left(\frac{m\ell}{M}-\frac{nk}{N}\right)}. \quad (14)$$

It can be shown that $y^{(p^*,q)}_{k,\ell}$ can be written as in (15), as shown at the bottom of the next page, where $\Psi^{(p,q')}_{k,k',\ell,\ell'}(\tau_{p,q},\nu_{p,q})$ is given in (16).

Stacking all the symbols received by the q-th UT from the p^*-th satellite in the NM-dimensional vector $\mathbf{y}^{(p^*,q)}$ and the symbols intended to the q-th UT in the NM-dimensional vector $\mathbf{x}^{(q)}$, we can write the whole observable as in (17), as shown at the bottom of the p. 8, where the $(kM+\ell+1,k'M+\ell'+1)$-th entry of the $NM\times NM$-dimensional matrix $\mathbf{\Psi}^{(p,q)}$ is

$$\mathbf{\Psi}_{p,q}(kM+\ell+1,k'M+\ell'+1) = \Psi^{(p,q)}_{k,k',\ell,\ell'}(\tau_{p,q},\nu_{p,q}), \quad (18)$$

with $k=0,\ldots,N-1$ and $\ell=0,\ldots,M-1$.

C. OFDM SIGNAL MODEL

Consider now a standard OFDM modulation with cyclic prefix (CP) in order to avoid the inter-symbol interference (ISI) and denote by $x^{(q)}_{n,m}$ the information symbol on the m-th subcarrier in the n-th symbol intended to the q-th UT belonging to a QAM constellation. The resulting OFDM symbol duration is $T_0 = T_{\mathrm{CP}}+T$, where T_{CP} and T denote the duration of CP and data symbols, respectively.

The continuous-time OFDM transmitted signal with CP at the p-th satellite is the following N_{S}-dimensional continuous time function

$$\mathbf{s}_p(t) = \sum_{q=0}^{Q-1}\alpha_{p,q}\sqrt{\eta_{p,q}}\mathbf{w}_{p,q}\sum_{n=0}^{N-1}\sum_{m=0}^{M-1}x^{(q)}_{n,m}$$
$$\times \mathrm{rect}(t-nT)e^{j2\pi m\Delta_f(t-nT_0-T_{\mathrm{CP}})}, \quad (19)$$

with all the quantities defined as in (5).

The signal received at the q-th UE to detect the information transmitted from the p^*-th satellite can be written as in (7) where now substituting the expression of $\mathbf{s}_p(t)$ in (19) and after some manipulations we obtain

$$r_{p^*,q}(t) = \sum_{p=0}^{P-1}\rho_{p,q}\mathbf{v}^T_{p^*,q}\mathbf{a}_{\mathrm{UT}}\left(\phi^{\mathrm{UT}}_{p,q},\theta^{\mathrm{UT}}_{p,q}\right)\mathbf{a}^T_{\mathrm{S}}\left(\phi^{\mathrm{S}}_{p,q},\theta^{\mathrm{S}}_{p,q}\right)$$
$$\times \sum_{q'=0}^{Q-1}\alpha_{p,q'}\sqrt{\eta_{p,q'}}\mathbf{w}_{p,q'}\sum_{n'=0}^{N-1}\sum_{m'=0}^{M-1}x^{(q')}_{n',m'}$$
$$\times \mathrm{rect}\left(t-n'T_0-T_{\mathrm{CP}}-\tau_{p,q}\right)$$
$$\times e^{j2\pi m'\Delta_f(t-n'T-\tau_{p,q})}e^{j2\pi\nu_{p,q}t} + \mathbf{v}^T_{p^*,q}\mathbf{z}_q(t). \quad (20)$$

By sampling every T/M and removing the CP in each OFDM symbol, we obtain

$$r^{(p^*,q)}_{n,m} = r_{p^*,q}(t)|_{t=nT_0+T_{\mathrm{CP}}+mT/M}$$
$$= \sum_{p=0}^{P-1}\rho_{p,q}\mathbf{v}^T_{p^*,q}\mathbf{a}_{\mathrm{UT}}\left(\phi^{\mathrm{UT}}_{p,q},\theta^{\mathrm{UT}}_{p,q}\right)\mathbf{a}^T_{\mathrm{S}}\left(\phi^{\mathrm{S}}_{p,q},\theta^{\mathrm{S}}_{p,q}\right)$$

$$r_{p^*,q}(t) = \sum_{p=0}^{P-1}\rho_{p,q}\mathbf{v}^T_{p^*,q}\mathbf{a}_{\mathrm{UT}}\left(\phi^{\mathrm{UT}}_{p,q},\theta^{\mathrm{UT}}_{p,q}\right)\mathbf{a}^T_{\mathrm{S}}\left(\phi^{\mathrm{S}}_{p,q},\theta^{\mathrm{S}}_{p,q}\right)\sum_{q'=0}^{Q-1}\alpha_{p,q'}\sqrt{\eta_{p,q'}}\mathbf{w}_{p,q'}\times$$
$$\sum_{n'=0}^{N-1}\sum_{m'=0}^{M-1}X^{(q')}_{n',m'}g_{TX}(t-n'T-\tau_{p,q})e^{j2\pi m'\Delta_f(t-n'T-\tau_{p,q})}e^{j2\pi\nu_{p,q}t} + \mathbf{v}^T_{p^*,q}\mathbf{z}_q(t) \quad (8)$$

$$\times \sum_{q'=0}^{Q-1} \alpha_{p,q'} \sqrt{\eta_{p^*,q'}} e^{j2\pi n T_0 \nu_{p,q}} \mathbf{w}_{p,q'} \times \sum_{m'=0}^{M-1} x_{n,m'}^{(q')} e^{j2\pi \frac{m}{M}\left(\frac{\nu_{p,q}}{\Delta_f}+m'\right)} e^{-j2\pi m' \Delta_f \tau_{p,q}} + z_{n,m}^{(p^*,q)}, \quad (21)$$

with $z_{n,m}^{(p^*,q)} = \mathbf{v}_{p^*,q}^T \mathbf{z}_{n,m}^{(q)}$, and $\mathbf{z}_{n,m}^{(q)}$ the sampled version of $\mathbf{z}_q(t)$.

Finally, the received signal is FFTed as

$$y_{n,m}^{(p^*,q)} = \frac{1}{M} \sum_{i=0}^{M-1} r_{n,i}^{(p^*,q)} e^{-j2\pi \frac{mi}{M}}. \quad (22)$$

It can be shown that $y_{n,m}^{(p^*,q)}$ can be written as in (23), as shown at the bottom of the next page, where $\Psi_{m,m',n}^{(p,q')}(\tau_{p,q}, \nu_{p,q})$ is reported in (24), as shown at the bottom of the next page.

Stacking all the symbols received by the q-th UT from the p^*-th satellite in the NM-dimensional vector $\mathbf{y}^{(p^*,q)}$ and the symbols intended to the q-th UT in the NM-dimensional vector $\mathbf{x}^{(q)}$, we can write the whole observable at the q-th UT as in (25), as shown at the bottom of the p. 9, where the $NM \times NM$-dimensional matrix $\mathbf{\Psi}_{p,q}$ is obtained as follows

$$\mathbf{\Psi}_{p,q} = \text{blkdiag}\left(\widetilde{\mathbf{\Psi}}_1^{(p,q)}, \ldots, \widetilde{\mathbf{\Psi}}_N^{(p,q)}\right), \quad (26)$$

where the (m, m')-th entry of the M-dimensional matrix $\widetilde{\mathbf{\Psi}}_n^{(p,q)}$ is

$$\widetilde{\mathbf{\Psi}}_n^{(p,q)}(m, m') = \Psi_{m,m',n}^{p,q}(\tau_{p,q}, \nu_{p,q}). \quad (27)$$

III. RECEIVER POST-PROCESSING

In both OFDM and OTFS, the whole observable at the q-th UT from the p^*-th satellite, $\mathbf{y}^{(p^*,q)}$ say, obtained by stacking $y_{n,m}^{(p^*,q)}$, $\forall n = 0, \ldots, N-1$, $m = 0, \ldots, M-1$ for OFDM and $y_{k,\ell}^{(p^*,q)}$, $\forall k = 0, \ldots, N-1$, $\ell = 0, \ldots, M-1$ for OTFS, can be expressed as

$$\mathbf{y}^{(p^*,q)} = \underbrace{\alpha_{p^*,q}\sqrt{\eta_{p^*,q}}\mu_{p^*,p^*,q,q}\mathbf{\Psi}_{p^*,q}\mathbf{x}^{(q)}}_{\text{intended signal to the } q\text{-th UT from the } p^*\text{-th satellite}} + \underbrace{\sum_{\substack{p=0 \\ p\neq p^*}}^{P-1} \alpha_{p,q}\sqrt{\eta_{p,q}}\mu_{p^*,p,q,q}\mathbf{\Psi}_{p,q}\mathbf{x}^{(q)}}_{\text{intended signal to the } q\text{-th UT from the other satellites}} + \underbrace{\sum_{p=0}^{P-1}\sum_{\substack{q'=0 \\ q'\neq q}}^{Q-1} \alpha_{p,q'}\sqrt{\eta_{p,q'}}\mu_{p^*,p,q,q'}\mathbf{\Psi}_{p,q}\mathbf{x}^{(q')}}_{\text{interference from the other downlink transmissions}} + \underbrace{\mathbf{z}^{(p^*,q)}}_{\text{noise}},$$

where the $NM \times NM$-dimensional matrix $\mathbf{\Psi}_{p,q}$ depends on the processing: for OTFS it is defined in (18) and for OFDM in (26). We defined the auxiliary variable $\mu_{p^*,p,q,q'}$ for OTFS and OFDM, respectively, as

$$\mu_{p^*,p,q,q'} = \widetilde{\rho}_{p,q}\mathbf{v}_{p^*,q}^T\mathbf{a}_{\text{UT}}\left(\phi_{p,q}^{\text{UT}}, \theta_{p,q}^{\text{UT}}\right)\mathbf{a}_{\text{S}}^T\left(\phi_{p,q}^{\text{S}}, \theta_{p,q}^{\text{S}}\right)\mathbf{w}_{p,q'},$$
$$\mu_{p^*,p,q,q'} = \rho_{p,q}\mathbf{v}_{p^*,q}^T\mathbf{a}_{\text{UT}}\left(\phi_{p,q}^{\text{UT}}, \theta_{p,q}^{\text{UT}}\right)\mathbf{a}_{\text{S}}^T\left(\phi_{p,q}^{\text{S}}, \theta_{p,q}^{\text{S}}\right)\mathbf{w}_{p,q'}. \quad (28)$$

Upon defining $\mathcal{S}_q : \{p^* : \alpha_{p^*,q} = 1\}$ as the set containing the serving satellites for the q-th UT, the estimation of the symbols intended for the q-th UT can be obtained by summing the contributions from the serving satellites:

$$\widehat{\mathbf{y}}^{(q)} = \sum_{p^*\in\mathcal{S}_q} \mathbf{y}^{(p^*,q)}. \quad (29)$$

Using a compact notation, we can write (29) as

$$\widehat{\mathbf{y}}^{(q)} = \mathbf{A}_q\mathbf{x}^{(q)} + \mathbf{B}_q\mathbf{x}^{(q)} + \sum_{\substack{q'=0 \\ q'\neq q}}^{Q-1}\mathbf{C}_{q,q'}\mathbf{x}^{(q')} + \mathbf{N}_q\overline{\mathbf{z}}^{(q)} \quad (30)$$

with

$$\mathbf{A}_q = \sum_{p^*\in\mathcal{S}_q}\sqrt{\eta_{p^*,q}}\mu_{p^*,p^*,q,q}\mathbf{\Psi}_{p^*,q}$$
$$\mathbf{B}_q = \sum_{p^*\in\mathcal{S}_q}\sum_{\substack{p=0 \\ p\neq p^*}}^{P-1}\alpha_{p,q}\sqrt{\eta_{p,q}}\mu_{p^*,p,q,q}\mathbf{\Psi}_{p,q}$$
$$\mathbf{C}_{q,q'} = \sum_{p^*\in\mathcal{S}_q}\sum_{p=0}^{P-1}\alpha_{p,q'}\sqrt{\eta_{p,q'}}\mu_{p^*,p,q,q'}\mathbf{\Psi}_{p,q}$$
$$\mathbf{N}_q = \sum_{p^*\in\mathcal{S}_q}\mathbf{I}_{NM}\otimes\mathbf{v}_{p^*,q}^T \quad (31)$$

and $\overline{\mathbf{z}}^{(q)} \sim \mathcal{CN}(\mathbf{0}_{NMN_{\text{UT}}}, \sigma_z^2\mathbf{I}_{NMN_{\text{UT}}})$ the vector containing the N_{UT}-dimensional subvectors $\overline{\mathbf{Z}}_{m,n}^{(q)}$, $\forall m, n$.

We assume that the q-th UT in order to detect the information symbols stacked in the vector $\mathbf{x}^{(q)}$ applies a

$$y_{k,\ell}^{(p^*,q)} = \sum_{p=0}^{P-1}\alpha_{p,q}\sqrt{\eta_{p,q}}\widetilde{\rho}_{p,q}\mathbf{v}_{p^*,q}^T\mathbf{a}_{\text{UT}}\left(\phi_{p,q}^{\text{UT}}, \theta_{p,q}^{\text{UT}}\right)\mathbf{a}_{\text{S}}^T\left(\phi_{p,q}^{\text{S}}, \theta_{p,q}^{\text{S}}\right)\mathbf{w}_{p,q}\sum_{k'=0}^{N-1}\sum_{\ell'=0}^{M-1}x_{k',\ell'}^{(q)}\Psi_{k,k',\ell,\ell'}^{(p,q)}(\tau_{p,q}, \nu_{p,q})$$
$$+ \sum_{p=0}^{P-1}\sum_{\substack{q'=0 \\ q'\neq q}}^{Q-1}\alpha_{p,q'}\sqrt{\eta_{p,q'}}\widetilde{\rho}_{p,q}\mathbf{v}_{p^*,q}^T\mathbf{a}_{\text{UT}}\left(\phi_{p,q}^{\text{UT}}, \theta_{p,q}^{\text{UT}}\right)\mathbf{a}_{\text{S}}^T\left(\phi_{p,q}^{\text{S}}, \theta_{p,q}^{\text{S}}\right)\mathbf{w}_{p,q'}\sum_{k'=0}^{N-1}\sum_{\ell'=0}^{M-1}x_{k',\ell'}^{(q')}\Psi_{k,k',\ell,\ell'}^{(p,q)}(\tau_{p,q}, \nu_{p,q}) + z_{k,\ell}^{(p^*,q)} \quad (15)$$

$$\Psi_{k,k',\ell,\ell'}^{(p,q)}(\tau_{p,q}, \nu_{p,q}) = \frac{1}{NM}\sum_{n=0}^{N-1}\sum_{m=0}^{M-1}\sum_{n'=0}^{N-1}\sum_{m'=0}^{M-1}C_{n,n',m,m'}(\tau_{p,q}, \nu_{p,q})e^{j2\pi\left(\frac{n'k'}{N}-\frac{m'\ell'}{M}\right)}e^{-j2\pi\left(\frac{nk}{N}-\frac{m\ell}{M}\right)}. \quad (16)$$

"practical" MMSE detection.[2] More precisely, we focus on the following observable, i.e.,

$$\widehat{\mathbf{x}}^{(q)} = \mathbf{D}_q^H \widehat{\mathbf{y}}^{(q)}, \tag{32}$$

with $\widehat{\mathbf{y}}^{(q)}$ expressed according to (30) and we assume only the knowledge of the channels from the serving satellites at each UT, i.e., the MMSE estimator matrix $\mathbf{D}_q$ is obtained as

$$\mathbf{D}_q = \left[\mathbf{A}_q \mathbf{A}_q^H + \sigma_z^2 \mathbf{I}_{NM}\right]^{-1} \mathbf{A}_q. \tag{33}$$

Now, by defining $\ell = (n-1)M + m$, with $m = 1, \ldots, M$ and $n = 1, \ldots, N$, the expression of the generic ℓ-th symbol estimated at the q-th UT can be expressed as

$$\widehat{\mathbf{x}}^{(q)}(\ell) = \mathbf{D}_q^H(\ell, :)\mathbf{A}_q \mathbf{x}^{(q)} + \mathbf{D}_q^H(\ell, :)\mathbf{B}_q \mathbf{x}^{(q)} + \sum_{\substack{q'=0 \\ q' \neq q}}^{Q-1} \mathbf{D}_q^H(\ell, :)\mathbf{C}_{q,q'} \mathbf{x}^{(q')} + \mathbf{D}_q^H(\ell, :)\mathbf{N}_q \bar{\mathbf{z}}^{(q)}. \tag{34}$$

[2]In this paper, we are assuming perfect channel state information (PCSI). However, the channel parameters (path-loss, delay and Doppler shift) are here needed for the implementation of the receiver to detect the symbols and must be estimated only from the UTs on the downlink and not from the satellites. The literature on OTFS and OFDM offers efficient algorithms to perform the channel estimation and we can refer to the procedures in reference [31] that can be applied directly here on the signal received at the single UT.

Define $i = (n'-1)M + m'$, with $m' = 1, \ldots, M$ and $n' = 1, \ldots, N$, and note that

$$\overline{\mathbf{\Psi}}^{(p,q)} \mathbf{x}^{(q)} = \sum_{i=1}^{NM} \overline{\mathbf{\Psi}}^{(p,q)}(:, i)\mathbf{x}^{(q)}(i). \tag{35}$$

By using the definitions of $\mathbf{A}_q$, $\mathbf{B}_q$, and $\mathbf{C}_{q,q'}$ given in (31), the expression of the generic ℓ-th symbol estimated at the q-th UT can be expressed as in (36) at the bottom of the next page.

The main mathematical symbols used in this paper are summarized in Table 1.

IV. FURTHER SYSTEM DESIGN ASPECTS

In this section, we discuss further aspects of the system design, such as the choice of the beamforming and combining at the satellites and at the UTs, respectively, the power control policy and the association between satellites and UTs.

A. BEAMFORMING AND COMBINING DESIGN

For the design of the beamforming vectors at the satellites and of the combining vectors at the UTs, as a direct consequence of the consideration of relative delays and Doppler shifts as discussed in Section II-A, we assume some uncertainty on the knowledge of the UTs' position (at the satellites), and of the satellites' positions (at the UTs).[3]

[3]The performance of the system is affected from this uncertainty, both in terms of beam precision and in terms of channel estimation capability of the considered modulation format.

$$\begin{aligned}\mathbf{y}^{(p^*,q)} = & \underbrace{\alpha_{p^*,q}\sqrt{\eta_{p^*,q}}\widetilde{\rho}_{p^*,q}\mathbf{v}_{p^*,q}^T \mathbf{a}_{\mathrm{UT}}\left(\phi_{p^*,q}^{\mathrm{UT}}, \theta_{p^*,q}^{\mathrm{UT}}\right)\mathbf{a}_{\mathrm{S}}^T\left(\phi_{p^*,q}^{\mathrm{S}}, \theta_{p^*,q}^{\mathrm{S}}\right)\mathbf{w}_{p^*,q}\mathbf{\Psi}_{p^*,q}\mathbf{x}^{(q)}}_{\text{intended signal to the } q\text{-th UT from the } p^*\text{-th satellite}} \\ & + \underbrace{\sum_{\substack{p=0 \\ p\neq p^*}}^{P-1} \alpha_{p,q}\sqrt{\eta_{p,q}}\widetilde{\rho}_{p,q}\mathbf{v}_{p^*,q}^T \mathbf{a}_{\mathrm{UT}}\left(\phi_{p,q}^{\mathrm{UT}}, \theta_{p,q}^{\mathrm{UT}}\right)\mathbf{a}_{\mathrm{S}}^T\left(\phi_{p,q}^{\mathrm{S}}, \theta_{p,q}^{\mathrm{S}}\right)\mathbf{w}_{p,q}\mathbf{\Psi}_{p,q}\mathbf{x}^{(q)}}_{\text{intended signal to the } q\text{-th UT from the other satellites}} \\ & + \underbrace{\sum_{p=0}^{P-1}\sum_{\substack{q'=0 \\ q'\neq q}}^{Q-1} \alpha_{p,q'}\sqrt{\eta_{p,q'}}\widetilde{\rho}_{p,q}\mathbf{v}_{p^*,q}^T \mathbf{a}_{\mathrm{UT}}\left(\phi_{p,q}^{UE}, \theta_{p,q}^{\mathrm{UT}}\right)\mathbf{a}_{\mathrm{S}}^T\left(\phi_{p,q}^{\mathrm{S}}, \theta_{p,q}^{\mathrm{S}}\right)\mathbf{w}_{p,q'}\mathbf{\Psi}_{p,q}\mathbf{x}^{(q')} + \underbrace{\mathbf{z}^{(p^*,q)}}_{\text{noise}}}_{\text{interference from the other downlink transmissions}}\end{aligned} \tag{17}$$

$$\begin{aligned}y_{n,m}^{(p^*,q)} = & \sum_{p=0}^{P-1} \alpha_{p,q}\sqrt{\eta_{p,q}}\rho_{p,q}\mathbf{v}_{p^*,q}^T \mathbf{a}_{\mathrm{UT}}\left(\phi_{p,q}^{\mathrm{UT}}, \theta_{p,q}^{\mathrm{UT}}\right)\mathbf{a}_{\mathrm{S}}^T\left(\phi_{p,q}^{\mathrm{S}}, \theta_{p,q}^{\mathrm{S}}\right)\mathbf{w}_{p,q}\sum_{m'=0}^{M-1} x_{n,m'}^{(q)}\Psi_{m,m',n}^{(p,q)}\left(\tau_{p,q}, \nu_{p,q}\right) \\ & + \sum_{p=0}^{P-1}\sum_{\substack{q'=0 \\ q'\neq q}}^{Q-1} \alpha_{p,q'}\sqrt{\eta_{p,q'}}\rho_{p,q}\mathbf{v}_{p^*,q}^T \mathbf{a}_{\mathrm{UT}}\left(\phi_{p,q}^{\mathrm{UT}}, \theta_{p,q}^{\mathrm{UT}}\right)\mathbf{a}_{\mathrm{S}}^T\left(\phi_{p,q}^{\mathrm{S}}, \theta_{p,q}^{\mathrm{S}}\right)\mathbf{w}_{p,q'}\sum_{m'=0}^{M-1} x_{n,m'}^{(q')}\Psi_{m,m',n}^{(p,q)}\left(\tau_{p,q}, \nu_{p,q}\right) + z_{n,m}^{(p^*,q)}\end{aligned} \tag{23}$$

$$\Psi_{m,m',n}^{(p,q)}\left(\tau_{p,q}, \nu_{p,q}\right) = \frac{1}{M} e^{j2\pi n T_0 \nu_{p,q}} e^{-j2\pi m' \Delta_f \tau_{p,q}} \sum_{i=0}^{M-1} e^{j2\pi \frac{i}{M}\frac{\nu_{p,q}}{\Delta_f}} e^{j2\pi \frac{i}{M}(m'-m)} \tag{24}$$

For this purpose, we denote by $\overline{\phi}^{\mathrm{S}}_{p,q}, \overline{\theta}^{\mathrm{S}}_{p,q}$, the azimuth and elevation position of the q-th UT known by the p-th satellite, i.e., *approximate DoD* for the q-th UT, and by $\overline{\phi}^{\mathrm{UT}}_{p,q}, \overline{\theta}^{\mathrm{UT}}_{p,q}$, the azimuth and elevation position of the p-th satellite known by the q-th UT, i.e., *approximate DoA* for the q-th UT. The beamformer and combiner design is focused on the quantity

$$\mu_{p^*,p,q,q'} = \overline{\rho}_{p,q} \underbrace{\mathbf{v}^T_{p^*,q} \mathbf{a}_{\mathrm{UT}}\left(\phi^{\mathrm{UT}}_{p,q}, \theta^{\mathrm{UT}}_{p,q}\right)}_{\mathrm{UT}} \underbrace{\mathbf{a}^T_{\mathrm{S}}\left(\phi^{\mathrm{S}}_{p,q}, \theta^{\mathrm{S}}_{p,q}\right) \mathbf{w}^{(p,q')}}_{\mathrm{Satellite}}, \tag{37}$$

where $\overline{\rho}_{p,q} = \rho_{p,q}$ for OFDM and $\overline{\rho}_{p,q} = \widetilde{\rho}_{p,q}$ for OTFS. In the design of the combiner, we can assume that the UT takes care of the first part of $\mu_{p^*,p,q,q'}$, while in the design of the beamformer we can assume that the satellite takes care of the second part of $\mu_{p^*,p,q,q'}$, as detailed in (37).

In this work, when designing the beamforming and combining vectors, we only assume the knowledge of the approximate positions of satellites and UTs. We here detail the proposed approaches based on beam-focus (BF) and zero-forcing (ZF) approaches.[4]

We thus consider the following beamforming techniques:

- *Beam-focus beamforming (BFB)*: The p-th satellite uses a beam aligned to the approximate DoD for the q-th UT, i.e.,

$$\mathbf{w}^{(p,q)} = \frac{\mathbf{a}^*_{\mathrm{S}}\left(\overline{\phi}^{\mathrm{S}}_{p,q}, \overline{\theta}^{\mathrm{S}}_{p,q}\right)}{\left\|\mathbf{a}_{\mathrm{S}}\left(\overline{\phi}^{\mathrm{S}}_{p,q}, \overline{\theta}^{\mathrm{S}}_{p,q}\right)\right\|}. \tag{38}$$

- *Zero-forcing beamforming (ZFB)*: The p-th satellite, in designing the beamforming for the q-th UT, nulls the interference on the approximate DoD for other UTs, i.e.,

$$\mathbf{w}^{(p,q)} = \frac{\overline{\mathbf{w}}^*_{(p,q),\mathrm{ZF}}}{\|\overline{\mathbf{w}}_{(p,q),\mathrm{ZF}}\|}, \tag{39}$$

[4]Note that the consideration of more advanced beamforming and combining techniques, such as the regularized zero-forcing and MMSE leads to a performance improvement, but strongest assumptions are needed on the knowledge of the noise variance at the receiver and channel gains.

$$\begin{aligned}\mathbf{y}^{(p^*,q)} = {} & \underbrace{\alpha_{p^*,q}\sqrt{\eta_{p^*,q}}\rho_{p^*,q}\mathbf{v}^T_{p^*,q}\mathbf{a}_{\mathrm{UT}}\left(\phi^{\mathrm{UT}}_{p^*,q}, \theta^{\mathrm{UT}}_{p^*,q}\right)\mathbf{a}^T_{\mathrm{S}}\left(\phi^{\mathrm{S}}_{p^*,q}, \theta^{\mathrm{S}}_{p^*,q}\right)\mathbf{w}_{p^*,q}\boldsymbol{\Psi}_{p^*,q}\mathbf{x}^{(q)}}_{\text{intended signal to the } q\text{-th UT from the } p^*\text{-th satellite}} \\ & + \underbrace{\sum_{\substack{p=0 \\ p\neq p^*}}^{P-1} \alpha_{p,q}\sqrt{\eta_{p,q}}\rho_{p,q}\mathbf{v}^T_{p^*,q}\mathbf{a}_{\mathrm{UT}}\left(\phi^{\mathrm{UT}}_{p,q}, \theta^{\mathrm{UT}}_{p,q}\right)\mathbf{a}^T_{\mathrm{S}}\left(\phi^{\mathrm{S}}_{p,q}, \theta^{\mathrm{S}}_{p,q}\right)\mathbf{w}_{p,q}\boldsymbol{\Psi}_{p,q}\mathbf{x}^{(q)}}_{\text{intended signal to the } q\text{-th UT from the other satellites}} \\ & + \underbrace{\sum_{p=0}^{P-1}\sum_{\substack{q'=0 \\ q'\neq q}}^{Q-1} \alpha_{p,q'}\sqrt{\eta_{p,q'}}\rho_{p,q}\mathbf{v}^T_{p^*,q}\mathbf{a}_{\mathrm{UT}}\left(\phi^{\mathrm{UT}}_{p,q}, \theta^{\mathrm{UT}}_{p,q}\right)\mathbf{a}^T_{\mathrm{S}}\left(\phi^{\mathrm{S}}_{p,q}, \theta^{\mathrm{S}}_{p,q}\right)\mathbf{w}_{p,q'}\boldsymbol{\Psi}_{p,q}\mathbf{x}^{(q')}}_{\text{interference from the other downlink transmissions}} + \underbrace{\mathbf{z}^{(p^*,q)}}_{\text{noise}}\end{aligned} \tag{25}$$

$$\begin{aligned}\widehat{\mathbf{x}}^{(q)}(\ell) = {} & \underbrace{\sum_{p^*\in\mathcal{S}_q}\sqrt{\eta_{p^*,q}}\mu_{p^*,p^*,q,q}\mathbf{D}^H_q(\ell,:)\boldsymbol{\Psi}^{(p^*,q)}(:,\ell)\mathbf{x}^{(q)}(\ell)}_{\text{intended symbol}} + \underbrace{\sum_{\substack{i=1 \\ i\neq\ell}}^{NM}\sum_{p^*\in\mathcal{S}_q}\sqrt{\eta_{p^*,q}}\mu_{p^*,p^*,q,q}\mathbf{D}^H_q(\ell,:)\boldsymbol{\Psi}^{(p^*,q)}(:,i)\mathbf{x}^{(q)}(i)}_{\text{interference from other symbols intended to the } q\text{-th UT}} \\ & + \underbrace{\sum_{i=1}^{NM}\sum_{p^*\in\mathcal{S}_q}\sum_{\substack{p\in\mathcal{S}_q \\ p\neq p^*}}\sqrt{\eta_{p,q}}\mu_{p^*,p,q,q}\mathbf{D}^H_q(\ell,:)\boldsymbol{\Psi}^{(p,q)}(:,i)\mathbf{x}^{(q)}(i)}_{\text{interference from symbols intended to the } q\text{-th UT due to receiving beams mismatch}} \\ & + \underbrace{\sum_{\substack{q'=0 \\ q'\neq q}}^{Q-1}\sum_{i=1}^{NM}\sum_{p^*\in\mathcal{S}_q}\sum_{p\in\mathcal{S}_{q'}}\sqrt{\eta_{p,q'}}\mu_{p^*,p,q,q'}\mathbf{D}^H_q(\ell,:)\boldsymbol{\Psi}^{(p,q)}(\ell,i)\mathbf{x}^{(q')}(i)}_{\text{interference from other transmission}} + \underbrace{\mathbf{D}^H_q(\ell,:)\mathbf{N}_q\overline{\mathbf{z}}^{(q)}}_{\text{noise contribution}}\end{aligned} \tag{36}$$

TABLE 1. Meaning of the main mathematical symbols.

Symbol	Description
P, Q	number of total satellites and UTs
M, N	number of subcarriers and symbols for OTFS and OFDM
$N_{\mathrm{S}}, N_{\mathrm{UT}}$	number of antennas at the satellites and UTs
$\rho_{p,q}, \nu_{p,q}, \tau_{p,q}$	channel gain, Doppler shift and path delay between the p-th satellite and the q-th UT
$\mathbf{a}_{\mathrm{UT}}(\phi_{p,q}^{\mathrm{UT}}, \theta_{p,q}^{\mathrm{UT}})$	array response at the q-th UT corresponding to the AoA from the p-th satellite
$\mathbf{a}_{\mathrm{S}}(\phi_{p,q}^{\mathrm{S}}, \theta_{p,q}^{\mathrm{S}})$	array response at the p-th satellite corresponding to the AoD to the q-th UT
$\mathbf{H}_{p,q}(t,\tau)$	downlink time-varying channel between the q-th UT and the p-th satellite
$\mathbf{w}_{p,q}$	beamforming vector used at the p-th satellite to serve the q-th UT
$\mathbf{v}_{p^*,q}$	combining vector at the q-th UE used to detect the signal transmitted from the p^*-th satellite
$\alpha_{p,q}$	binary variable being 1 if the p-th satellite serves the q-th UT and 0 otherwise
$\mu_{p^*,p,q,q'}$	auxiliary variable involving the p-th and p^*-th satellites and the q-th and q'-th UTs defines as in (28)
$\mathbf{y}^{(p^*,q)}$	observable at the q-th UT from the p^*-th satellite
$\mathcal{S}_q$	set containing the serving satellites for the q-th UT
$\mathbf{x}^{(q)}$	information symbols intended for the q-th UT
$\widehat{\mathbf{y}}^{(q)}$	estimation of the symbols intended for the q-th UT
$\mathbf{\Psi}^{(p,q)}$	$NM \times NM$-dimensional matrix synthesizing the channel and the modulation transmission from the p-th satellite to the q-th UT

where

$$\overline{\mathbf{w}}_{(p,q),\mathrm{ZF}} = \left(\mathbf{I}_{N_{\mathrm{S}}} - \mathbf{A}_{p,q}^{\mathrm{orth}}\mathbf{A}_{p,q}^{\mathrm{orth},H}\right)\mathbf{a}_{\mathrm{S}}\left(\overline{\phi}_{p,q}^{\mathrm{S}}, \overline{\theta}_{p,q}^{\mathrm{S}}\right) \quad (40)$$

$\mathbf{A}_{p,q}^{\mathrm{orth}} = \mathrm{orth}(\mathbf{A}_{p,q})$ and $\mathbf{A}_{p,q}$ contains on the columns $[\mathbf{a}_{\mathrm{S}}(\overline{\phi}_{p,q'}^{\mathrm{S}}, \overline{\theta}_{p,q'}^{\mathrm{S}}) : q' \neq q]$.

Regarding the combining, we consider the following techniques:

- *Beam-focus combining (BFC)*: The q-th UT uses a beam aligned to the approximate DoA for the p^*-th satellite by including a phase compensation of the channel gain, i.e.,

$$\mathbf{v}^{(p^*,q)} = \frac{\mathbf{a}_{\mathrm{UT}}^*\left(\overline{\phi}_{p^*,q}^{\mathrm{UT}}, \overline{\theta}_{p^*,q}^{\mathrm{UT}}\right)}{\left\|\mathbf{a}_{\mathrm{UT}}\left(\overline{\phi}_{p^*,q}^{\mathrm{UT}}, \overline{\theta}_{p^*,q}^{\mathrm{UT}}\right)\right\|}. \quad (41)$$

- *Zero-forcing combining (ZFC)*: The q-th UT, in designing the combining for the p^*-th satellite, nulls the interference on the approximate DoA for other serving satellites by including a phase compensation of the channel gain, i.e.,

$$\mathbf{v}^{(p^*,q)} = \frac{\overline{\mathbf{v}}_{(p^*,q),\mathrm{ZF}}^*}{\|\overline{\mathbf{v}}_{(p^*,q),\mathrm{ZF}}\|}, \quad (42)$$

with

$$\overline{\mathbf{v}}_{(p^*,q),\mathrm{ZF}} = \left(\mathbf{I}_{N_{\mathrm{UT}}} - \mathbf{B}_{p^*,q}^{\mathrm{orth}}\mathbf{B}_{p^*,q}^{\mathrm{orth},H}\right)\mathbf{a}_{\mathrm{UT}}\left(\overline{\phi}_{p^*,q}^{\mathrm{UT}}, \overline{\theta}_{p^*,q}^{\mathrm{UT}}\right) \quad (43)$$

$\mathbf{B}_{p^*,q}^{\mathrm{orth}} = \mathrm{orth}(\mathbf{B}_{p^*,q})$ and $\mathbf{B}_{p^*,q}$ contains on the columns $[\mathbf{a}_{\mathrm{UT}}(\overline{\phi}_{p,q}^{\mathrm{UT}}, \overline{\theta}_{p,q}^{\mathrm{UT}}) : p \neq p^* \text{ and } \alpha_{p,q} = 1]$.

B. POWER ALLOCATION AND UT-SATELLITE ASSOCIATION

Regarding the definition of the transmit power coefficients, we assume that each satellite uniformly distributes the available power budget to the UTs that it serves. In particular, denoting by $P_{p,\mathrm{SAT}}$ the total power available at the p-th satellite, the coefficients $\eta^{(p,q)}$ are expressed as:

$$\eta^{(p,q)} = \frac{\alpha_{p,q}P_{p,\mathrm{SAT}}}{MN\sum_{q=1}^{Q}\alpha_{p,q}}. \quad (44)$$

For the definition of the binary association variables $\alpha_{p,q}$, we consider the UC-CF approach [15]. Specifically, the q-th UT is served by the N_{UC} closest satellites. In particular, let $O_q : \{1,\ldots,P\} \to \{1,\ldots,P\}$ denote the sorting operator for the vector $[\overline{s}_{1,q}|, \ldots, |\overline{s}_{P,q}]$, with $\overline{s}_{p,q}$ the slant range between the q-th UT and the p-th satellite, such that

$$\overline{s}_{O_q(1),q} \leq \overline{s}_{O_q(2),q} \leq \ldots \leq \overline{s}_{O_q(P),q}. \quad (45)$$

We consider some *constraints* in the UT-satellite association in order to avoid overloading the satellites and reduce high mutual interference between UTs served by the same satellite. In particular, the following cases are considered:

- C_0: Each UT is served by the N_{UC} closest satellites, i.e., the binary association variables are defined as:

$$\begin{cases} \alpha_{O_q(1),q} = \ldots = \alpha_{O_q(N_{\mathrm{UC}}),q} = 1, \\ \alpha_{O_q(N_{\mathrm{UC}}+1),q} = \ldots = \alpha_{O_q(P),q} = 0 \end{cases}. \quad (46)$$

- C_1: Each UT is served by the N_{UC} closest satellites and the satellites must satisfy the restriction on the maximum number of UTs served, $N_{\mathrm{UT,MAX}}$ say.
- C_2: Each UT is served by the N_{UC} closest satellites and the satellites must satisfy a restriction on the minimum angular distance, δ say, between the served UTs.
- C_3: Each UT is served by the N_{UC} closest satellites and the satellites must satisfy the restriction on $N_{\mathrm{UT,MAX}}$ and δ.

In particular, in cases C_1, C_2, C_3, for the q-th UT with $q = 1,\ldots,Q$, we sort the satellites according to the sorting operator O_q in (45) and then select the closest N_{UC}

satellites satisfying the restrictions in terms of load and/or minimum angular distance between the served UTs. It is worth noting that for certain UTs, it may not always be possible to identify N_{UC} satellites meeting all constraints. Therefore, N_{UC} generally represents the maximum number of satellites that can serve each UT. Numerical simulations indicate that, in the considered scenario and for $N_{\mathrm{UC}} \in [1, 6]$ the probability of not finding N_{UC} suitable satellites for a given UT is very low. The constraints considered here are designed to reduce satellite complexity (C_1, by limiting the number of simultaneously served UTs) and to mitigate downlink inter-UT interference (C_2, by constraining the angular separation between UTs served by the same satellite). Practically, satellites require only the UTs' approximate positions, from which angular separations can be computed, and the maximum load each satellite can support, defined as a system design parameter.

V. PERFORMANCE ASSESSMENT

In the following, we illustrate the considered performance measures, the simulation setup, the specific model used for channel generation, and, finally, discuss the obtained numerical results.

A. PERFORMANCE MEASURES

The schemes developed in this paper will be assessed in terms of SINR and *pragmatic capacity*, which are defined next.

Starting from (36), the SINR on the ℓ-th symbol at the q-th UT is expressed as in (47) at the bottom of this page, obtained again by averaging on symbols and noise realizations.

Regarding instead the *pragmatic capacity* [31], we recall that is defined as the mutual information of the virtual channel with constellation symbols as input (uniformly distributed) and received samples after the MMSE processing as soft-outputs. This measure basically provides the achievable rate in the case of separated detection and decoding. Thus, given inputs $\mathbf{x}^{(q)}$ and outputs $\widehat{\mathbf{x}}^{(q)}$, the constellation $\mathcal{C}$ and the set of transmitted symbols, excluding the pilots, $\mathcal{D}$ (i.e., $|\mathcal{D}| \leq NM$), the pragmatic capacity for q-th UT can be derived as

$$I_{\mathrm{PC}} = \log_2 |\mathcal{C}| - \frac{1}{NM} \sum_{k \in \mathcal{D}} P(x_k, \widehat{x}_k) \log_2 \frac{1}{P(x_k|\widehat{x}_k)} \tag{48}$$

where $P(x_k|\widehat{x}_k)$ is the *a-posteriori* probability of symbols x_k given the detector soft-outputs $\widehat{x}_k$, whereas $P(x_k, \widehat{x}_k)$ is the joint probability function.

B. SIMULATION SETUP AND CHANNEL GENERATION

Results are provided taking as a case study a constellation similar to the Starlink LEO satellite mega-constellation. As of September 2024, the Space-X Starlink satellite constellation is the largest LEO operational satellite network, having already more than seven thousand satellites in orbit among different shells mainly at 445, 475, 485, 540, 550, 560, 560 and 570 km altitude, and over orbital planes with inclinations of 53°, 43°, 70° and 97.67° mainly. Starlink is planned to use inter-satellite links, even if not from the beginning, and the frequency usage will be in Ka and Ku bands.

The simulated scenario envisaged an observed fixed UT[5] surrounded by 50 interfering UTs randomly placed in a radius of 670 km, each with an estimated positioning offset (therefore the satellite delay and Doppler precompensation includes a residual error). The offset distance $r_{p,q}$ from the exact UT position was set as a random point within a circle of radius 500 meters $\forall p, q$. Six hundreds snapshots of the scenario were taken every second, and for each snapshot a new occurrence of interfering UTs positions was generated, and then 1-sec time-series sampled every 10 ms (i.e., 100 samples were taken, ideally emulating the state of the channel over the duration of one NR frame period, which is 10 ms) were used to simulate a narrowband flat-fading channel on each UT-satellite link. Concerning the waveform, the carrier frequency was set to $f = 20$ GHz (Ka-band), the subcarrier spacing to $\Delta f = 120$ kHz, the symbol time to $T = 8.33$ μs, with $M = 32$ and $N = 16$. The power spectral density of the noise was $N_0 = -174$ dBm/Hz and the noise figure at the receiver was $F = 5$ dB. We assumed $N_{S,X} = N_{S,Y} = 16$, i.e., $N_{\mathrm{S}} = 256$, $\Gamma_{\mathrm{SAT}} = 23$ dB at the satellites, and $N_{\mathrm{UT},X} = N_{\mathrm{UT},Y} = 4$, i.e., $N_{\mathrm{UT}} = 16$, $\Gamma_{\mathrm{UT}} = 10$ dB at the UTs. We assume that all the satellites have the same power budget, i.e., $P_{p,\mathrm{SAT}} = P_{\mathrm{SAT}}$, $\forall p = 1, \ldots, P$. The main simulation parameters are summarized in Table 2.

Given the described satellite scenario, the propagation channel is modeled following the two-state semi-Markov

[5]The geographic coordinates of the location were 47°33'33.6"N 7°35'22.8"E.

$$\overline{\gamma}^{(q)}(\ell) = \frac{\left| \sum_{p^* \in \mathcal{S}_q} \sqrt{\eta_{p^*,q}} \mu_{p^*,p^*,q,q} \mathbf{D}_q^H(:,\ell) \boldsymbol{\Psi}^{(p^*,q)}(:,\ell) \right|^2}{\left\{ \begin{array}{l} \sum_{\substack{i=1 \\ i \neq \ell}}^{NM} \left| \sum_{p^* \in \mathcal{S}_q} \sqrt{\eta_{p^*,q}} \mu_{p^*,p^*,q,q} \mathbf{D}_q^H(:,\ell) \boldsymbol{\Psi}^{(p^*,q)}(:,i) \right|^2 + \sum_{i=1}^{NM} \left| \sum_{p^* \in \mathcal{S}_q} \sum_{\substack{p \in \mathcal{S}_q \\ p \neq p^*}} \sqrt{\eta_{p,q}} \mu_{p^*,p,q,q} \mathbf{D}_q^H(:,\ell) \boldsymbol{\Psi}^{(p,q)}(:,i) \right|^2 \\ + \sum_{\substack{q'=0 \\ q' \neq q}}^{Q-1} \sum_{i=1}^{NM} \left| \sum_{p^* \in \mathcal{S}_q} \sum_{p \in \mathcal{S}_{q'}} \sqrt{\eta_{p,q'}} \mu_{p^*,p,q,q'} \mathbf{D}_q^H(:,\ell) \overline{\boldsymbol{\Psi}}^{(p,q)}(:,i) \right|^2 + \sigma_z^2 \left\| \mathbf{D}_q^H(:,\ell) \mathbf{N}_q \right\|^2 \end{array} \right\}} \tag{47}$$

TABLE 2. Simulation parameters.

Description	Value
Carrier frequency	20 GHz (Ka-band)
Subcarrier spacing, Symbol Time	120 kHz, 8.3 μs
Number of subcarriers, M	32
Number of symbols, N	16
PSD of noise, noise figure	-174 dBm/Hz, 5 dB
Number of UTs and number of satellites	$Q = 51$, $P = 6022$
Number of Antennas at the satellites, N_{S}	256, 16 $\times$ 16 UPA
Number of Antennas at the UT, N_{UT}	16, 4 $\times$ 4 UPA
Offset distance, $r_{p,q}$	500 m (maximum)
Satellite Constellation	Space-X Starlink
Large-scale propagation channel model	[43]

TABLE 3. ITU-R P.681-11 channel parameters for highway environment.

Parameter	GOOD	BAD
$\mu_{\mathrm{G,B}}$, $\sigma_{\mathrm{G,B}}$ (m)	1.27, 1.86	-0.31, 1.35
$dur_{\mathrm{minG,B}}$ (m)	0.01	0.5
$\mu_{\mathrm{M_A,G,B}}$, $\sigma_{\mathrm{M_A,G,B}}$ (dB)	-0.16, 0.39	-5.92, 8.20
$h_{1G,B}, h_{2G,B}$ (dB)	0.0, -29.61	-0.34, -14.39
$g_{1\mathrm{G,B}}, g_{2\mathrm{G,B}}$	0.0, 0.39	-0.41, 0.0
$L_{\mathrm{corrG,B}}$ (m)	0.15, 1.28	
$f_1\Delta\mathrm{M_A} + f_2$ (m)	[0.001, 0.861]	

model described in ITU-R Recommendation P.681-11 [42], with particular reference to the parameters for the highway environment reported in Table 3, specific for 20 GHz carrier frequency and for an elevation of 30 degrees. In the table, G,B stand for GOOD and BAD states, parameter (μ, σ) refers to the mean and standard deviation of the log-normal law assumed for events duration, $dur_{\mathrm{minG,B}}$ refers to the minimum possible events duration, $(\mu_{\mathrm{M_AG,B}}, \sigma_{\mathrm{M_AG,B}})$ to the mean and st. deviation of the average direct path amplitude ($\mathrm{M_A}$) over one event, $(h_{1G,B}, h_{2G,B})$ to the multipath power, $(g_{1\mathrm{G,B}}, g_{2\mathrm{G,B}})$ to the st. deviation of $\mathrm{M_A}$, $L_{\mathrm{corrG,B}}$ to the direct path amplitude correlation distance, $f_1\Delta\mathrm{M_A} + f_2$ to the transition length (being $\Delta\mathrm{M_A}$ the difference between $\mathrm{M_{AG}}$ and $\mathrm{M_{AB}}$). The choice of such a model is motivated by the fact that for transmissions in Ka-band with directive antennas a narrow-band (flat-fading) channel can be assumed. Also, uncorrelated links were assumed as satellites serving the same user are spatially separated both in terms of distance (hundreds or thousands of km) and angles of arrival.[6] Delays and Doppler shifts are computed for each satellite based on its true orbital speed and position, whereas a random speed in the range 50-130 km/s is assumed for each UT for each snapshot.

[6]The assumption of no correlation is also motivated by the Highway scenario here considered. In such propagation model, the typical obstacles are panels, poles and trees on the side of the road, therefore the signals transmitted by different satellites would likely experience independent blockage. In general, this assumption could entail slightly optimistic results, but, on the other hand, an exhaustive, reliable and realistic correlation model for LEO satellite scenarios in Ka band and open space is not available.

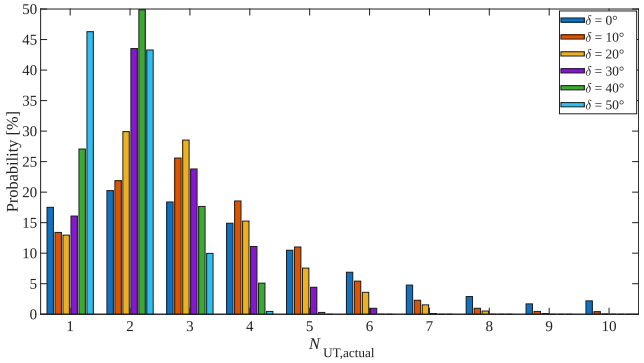

FIGURE 2. Distribution of the number of UTs served by each satellite over the ten minutes time span (with $N_{\mathrm{UT,MAX}} = 10$, $N_{\mathrm{UT,MAX}}$ being the maximum number of UTs served from each satellite), by considering the constraint C_2 with δ denoting the minimum angular distance between UTs served by the same satellite.

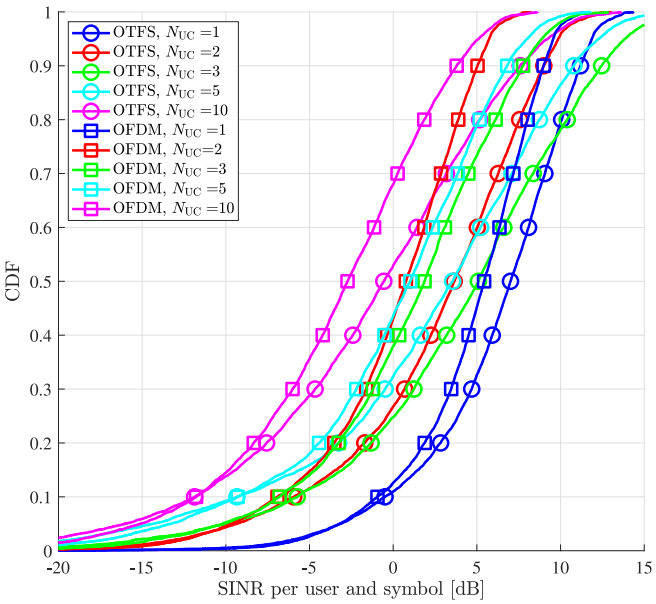

FIGURE 3. CDF of the SINR per user and symbol for OFDM and OTFS for different values of N_{UC} being the number of satellites serving each user, ZFB and $N_{\mathrm{UT}} = 1$, with N_{UT} denoting the number of antennas at the UTs, transmit power at the satellite $P_{\mathrm{SAT}} = 15$ dBW, and C_1 with $N_{\mathrm{UT,MAX}} = 10$, $N_{\mathrm{UT,MAX}}$ being the maximum number of UTs served from each satellite.

C. NUMERICAL RESULTS

Figure 2 shows how the distribution of the number of UTs served by the same satellite (which is in any case limited to 10), $N_{\mathrm{UT,actual}}$ say, changes when the constraint C_2 on the minimum angular distance is varied from 0° (no constraint) to 50°. It is then possible to notice that a higher angle constraint entails a higher percentage of few UTs served by the same satellite, thus obviously correlating the two constraints that cannot be considered as independent.

In Figures 3 and 4, we report the cumulative distribution functions (CDFs) of the SINR per user and symbol defined as in (47) in the case of single-antenna UTs and multiple antennas UTs, respectively, by assuming ZFB in both the figures and ZFC in Figure 4. We report the performance for different values of N_{UC} for both OTFS and OFDM. From Figure 3, it can be observed that, with single-antenna UTs

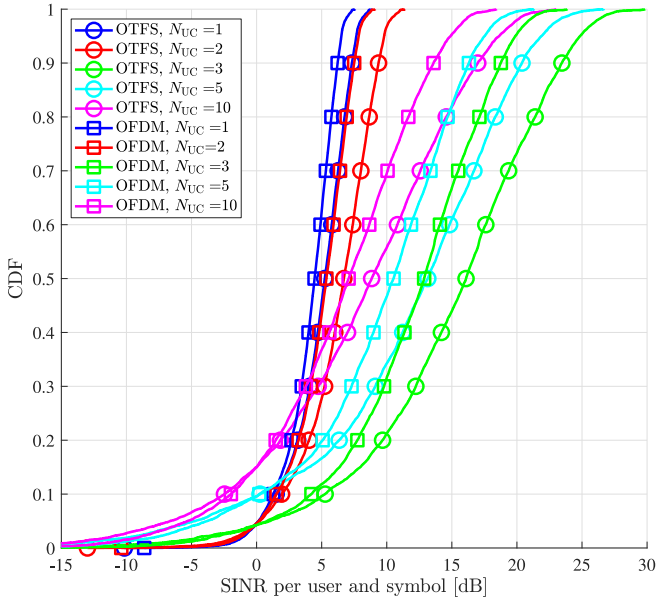

FIGURE 4. CDF of the SINR per user and symbol for OFDM and OTFS for different values of N_{UC} being the number of satellites serving each user, ZFB-ZFC and $N_{UT} = 16$, with N_{UT} denoting the number of antennas at the UTs, transmit power at the satellite $P_{SAT} = 15$ dBW, and C_1 with $N_{UT,MAX} = 10$, $N_{UT,MAX}$ being the maximum number of UTs served from each satellite.

and without phase compensation, the macro-diversity gains cannot be fully exploited. In this case, the signals from multiple serving satellites combine destructively, leading to a reduction in the useful signal power compared to the baseline ($N_{UC} = 1$). This behavior was also observed in reference [14], where we discussed that to exploit the benefits of macro-diversity, an at least coarse phase estimation of the channel must be used to perform a coherent joint transmission. However, in the case of multiple antennas UTs, shown in Figure 4, the use of ZFB and ZFC is able to isolate the contributions from different satellites and thus, thanks to the spatial filtering, we are able to exploit the benefits of the macro-diversity for the vast majority of the UTs. The comparison between OFDM and OTFS is also reported in terms of outage probability in Table 4 with a SINR target of 0 dB and a transmit power at the satellites of $P_{SAT} = 15$ dBW. We can observe that the performance considering single antennas UTs, i.e., $N_{UT} = 1$, is not acceptable in both cases, with a limited improvement in the case of OTFS while they are significantly improving considering multiple antennas UTs, i.e., $N_{UT} = 16$, and that the effectiveness of considering multi-satellite diversity is also observable in terms of system reliability.[7]

In Figure 5, we again report the CDFs of the SINR per user and symbol, focusing now only on the case $N_{UC} = 3$ with multiple antennas UTs, the one that achieves the best performance according to Figure 4, showing the impact of the beamforming and combining techniques used at the satellites and UTs. In particular, by inspecting the figure,

[7]Note that the last column of Table 4 refers to both OFDM and OTFS because of the overlap of the OFDM and OTFS SINR curves in the lower-left part of Figure 4.

TABLE 4. Outage probability with transmit power at the satellite $P_{SAT} = 15$ dBW, a SINR target of 0 dB with N_{UT} denoting the number of antennas at the UTs.

	OTFS, $N_{UT} = 1$	OFDM, $N_{UT} = 1$	$N_{UT} = 16$
$N_{UC} = 1$	11%	12.6%	4.6%
$N_{UC} = 2$	26.7%	43%	4.6%
$N_{UC} = 3$	24.7%	38%	4.2%
$N_{UC} = 5$	32.3%	43.5%	9.6%

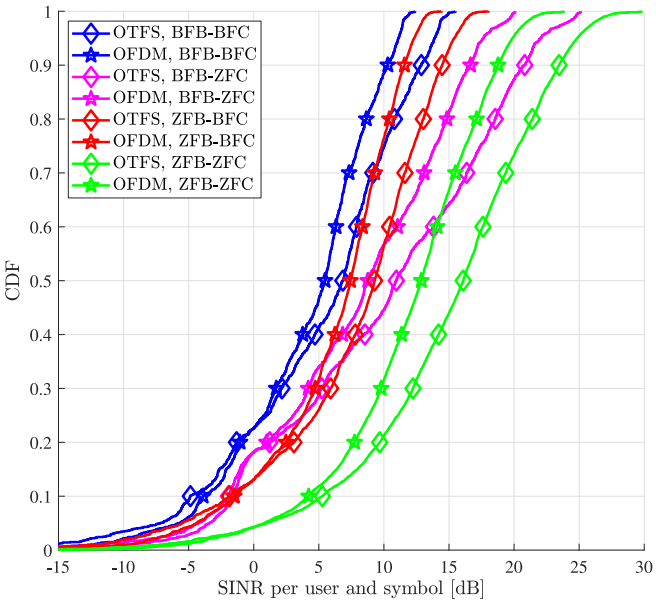

FIGURE 5. CDF of the SINR per user and symbol for OFDM and OTFS, $N_{UC} = 3$ being the number of satellites serving each user, transmit power at the satellite $P_{SAT} = 15$ dBW, C_1 with $N_{UT,MAX} = 10$, $N_{UT,MAX}$ being the maximum number of UTs served from each satellite, for different beamforming and combining techniques at the satellites and UTs.

we can observe that, as expected, the best performance is obtained in the case of ZF approaches aimed at nulling the interference in the directions corresponding to the approximate position of the interfering UTs and satellites. By comparing ZFB-BFC and BFB-ZFC curves in the lower left part of the figure we can observe that performing the ZF at the UTs is more effective than performing the ZF at the satellites in terms of fairness. In Figure 6, we show the CDFs of the SINR per user and symbol, focusing again on the case $N_{UC} = 3$ with multiple antennas UTs underlying the impact of the different UT-satellites association techniques. First, it can be observed that C_1, C_2 and C_3 outperform C_0. From the perspective of a generic satellite, limiting either the number of served UTs or the angular separation between them effectively allocates more power to fewer UTs, improving the utilization of available resources. Furthermore, C_2 and C_3 outperform C_1 because they select UTs based on their angular separation, which reduces downlink multi-user interference and consequently enhances the SINR per user and symbol.

Then, Figures 7 and 8 display the OTFS pragmatic capacity (without any pilot overheads) of the observed UT as a function of the transmitted power P_{SAT}, under constraint C_1 and C_2, respectively, for both QPSK and 16QAM modulation

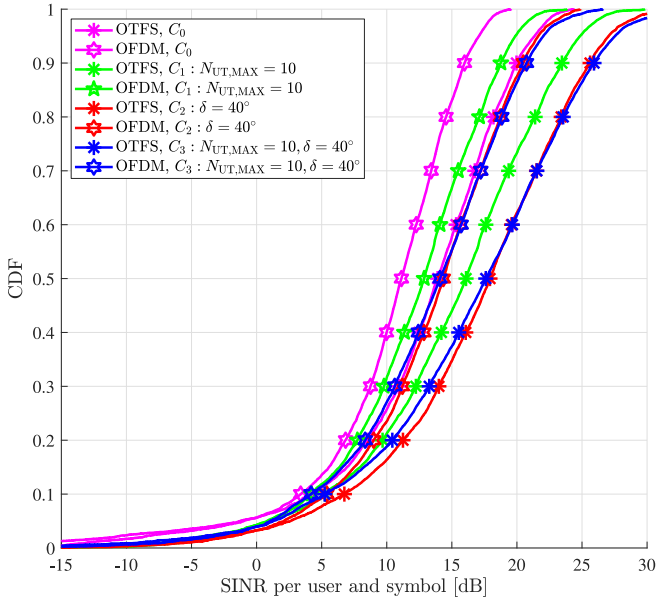

FIGURE 6. CDF of the SINR per user and symbol for OFDM and OTFS, $N_{\mathrm{UC}}=3$ being the number of satellites serving each user, ZFB-ZFC, transmit power at the satellite $P_{\mathrm{SAT}}=15$ dBW, for different UT-satellite association techniques. In the legend, $N_{\mathrm{UT,MAX}}$ represents the maximum number of UTs served from each satellite and δ denotes the minimum angular distance between UTs served by the same satellite.

formats[8] and with zero-forcing both at transmitter and receiver and $N_{\mathrm{UC}}=3$.

These results are in agreement with SINR results but provide a further insight on the impact of the constraints; the maximum number of served UTs entails a significant difference on the receiver performance when $N_{\mathrm{UT,MAX}}$ is greater than one, whereas, on the other hand, only a slight but uniform improvement can be noticed when the constraint on the minimum angle is increased from 0° (no constraint) to 40°. The same behavior is observed for both QPSK and 16QAM.

Finally, Figure 9 presents a comparison between a case where each UT is served by only one satellite and each satellite serves only one UT, i.e., $N_{\mathrm{UC}}=1$, $N_{\mathrm{UT,MAX}}=1$, $\delta=0°$ (briefly reported in the legend as $N_{\mathrm{UC}}=1$), and a case with $N_{\mathrm{UC}}=3$, $N_{\mathrm{UT,MAX}}=5$, $\delta=40°$ (briefly reported in the legend as $N_{\mathrm{UC}}=3$). In this case, the results are reported versus the normalized transmitted power $P_{\mathrm{SAT}*}$, computed from P_{SAT} by considering a constant penalty equal to the ratio of the average number or the respective employed satellites. This ratio, in the case of $N_{\mathrm{UC}}=3$, yields a value slightly higher than zero, since usually a few more satellites are used if the same UT is served by multiple satellites. For the scenario at hand, this power penalty was found to be 0.4 dB.[9] Therefore, it is evident that notable enhancements can be achieved in both pragmatic capacity and particularly in outage probability, as values as low as approximately 10% can be assured while saving power by roughly 5 dBW.

[8]Actually, only Figure 7 shows results on 16QAM because the behaviour was exactly the same when constraint C_2 was considered.

[9]Therefore, basically $P_{\mathrm{SAT}*}=P_{\mathrm{SAT}}+0.4$ dB in the case $N_{\mathrm{UC}}=3$ and $P_{\mathrm{SAT}*}=P_{\mathrm{SAT}}$ in the case $N_{\mathrm{UC}}=1$.

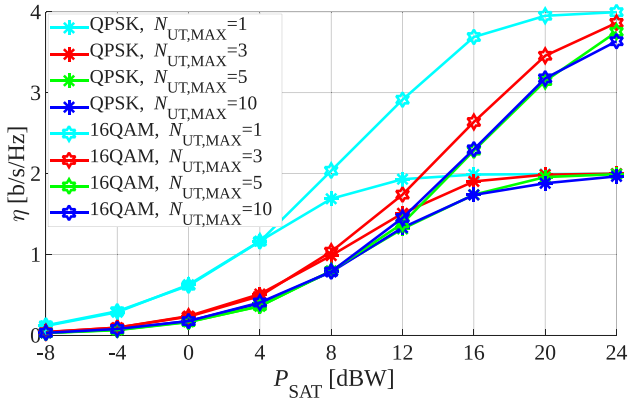

FIGURE 7. OTFS pragmatic capacity with $N_{\mathrm{UC}}=3$ being the number of satellites serving each user under constraint C_1, with $N_{\mathrm{UT,MAX}}$ being the maximum number of UTs served from each satellite.

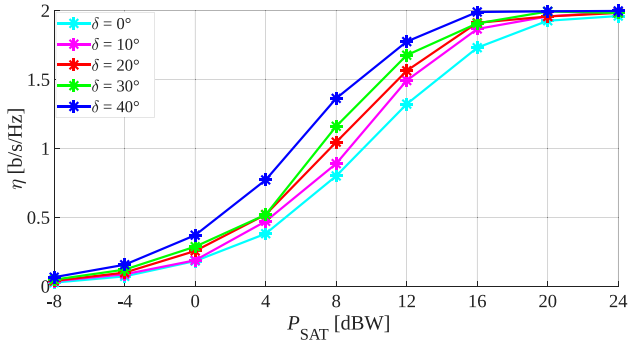

FIGURE 8. OTFS pragmatic capacity $N_{\mathrm{UC}}=3$ being the number of satellites serving each user under constraint C_2, with $N_{\mathrm{UT,MAX}}=20$, being the maximum number of UTs served from each satellite and δ denoting the minimum angular distance between UTs served by the same satellite.

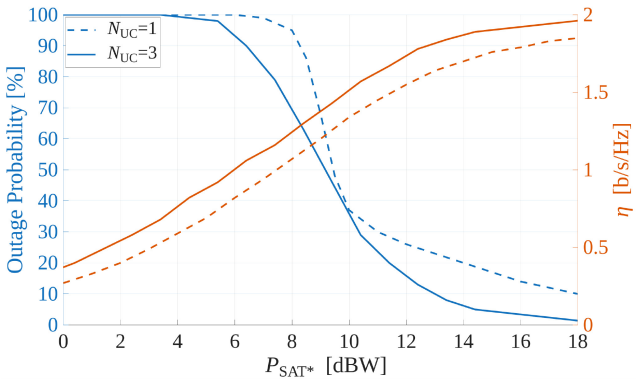

FIGURE 9. OTFS outage probability (left) and pragmatic capacity (right) as a function of the normalized transmitted power, comparison for two respective cases: a) $N_{\mathrm{UC}}=1$, $N_{\mathrm{UT,MAX}}=1$, $\delta=0°$; b) $N_{\mathrm{UC}}=3$, $N_{\mathrm{UT,MAX}}=5$, $\delta=40°$, where N_{UC} is the number of satellites serving each user, $N_{\mathrm{UT,MAX}}$ denotes the maximum number of UTs served from each satellite and δ denotes the minimum angular distance between UTs served by the same satellite.

VI. CONCLUSION

This paper has investigated macro-diversity strategies for LEO satellite systems, inspired by the principles of UC-CF massive MIMO. A comprehensive end-to-end transceiver model has been developed, accounting for Doppler shifts, phase offsets, and realistic waveform processing. Both

OFDM and OTFS modulation schemes have been considered, with OTFS demonstrating improved robustness under high mobility. The analysis has further explored multi-antenna UTs, showing that receive beamforming can effectively mitigate phase misalignment among signals from different satellites. Overall, the obtained results have confirmed that macro-diversity, when properly implemented, significantly enhances reliability and spectral efficiency in LEO-based non-terrestrial networks, and thus motivate further research on this subject. Future research efforts can be focused on considering the impact of Ricean-distributed propagation channels, integration with inter-satellite links, hybrid terrestrial-satellite coordination and resource scheduling under limited feedback.

ACKNOWLEDGMENT

The views expressed are those of the authors and do not necessarily represent the project. The Commission is not liable for any use that may be made of any of the information contained therein.

REFERENCES

[1] M. Giordani and M. Zorzi, "Non-terrestrial networks in the 6G era: Challenges and opportunities," *IEEE Netw.*, vol. 35, no. 2, pp. 244–251, Mar./Apr. 2021.

[2] M. M. Azari et al., "Evolution of non-terrestrial networks from 5G to 6G: A survey," *IEEE Commun. Surveys Tuts.*, vol. 24, no. 4, pp. 2633–2672, 4th Quart., 2022.

[3] T. Wei, W. Feng, Y. Chen, C.-X. Wang, N. Ge, and J. Lu, "Hybrid satellite-terrestrial communication networks for the maritime Internet of Things: Key technologies, opportunities, and challenges," *IEEE Internet Things J.*, vol. 8, no. 11, pp. 8910–8934, Jun. 2021.

[4] X. Fang, W. Feng, T. Wei, Y. Chen, N. Ge, and C.-X. Wang, "5G embraces satellites for 6G ubiquitous IoT: Basic models for integrated satellite terrestrial networks," *IEEE Internet Things J.*, vol. 8, no. 18, pp. 14399–14417, Sep. 2021.

[5] M. Harounabadi and T. Heyn, "Toward integration of 6G-NTN to terrestrial mobile networks: Research and standardization aspects," *IEEE Wireless Commun.*, vol. 30, no. 6, pp. 20–26, Dec. 2023.

[6] X. Tong, Z. Xie, and Y. Gu, "A review of non-terrestrial network standard development in 3GPP RAN and future directions for 6G," in *Proc. AIAA SCITECH Forum*, Jan. 2025, p. 2717.

[7] H. Xie, Y. Zhan, G. Zeng, and X. Pan, "LEO mega-constellations for 6G global coverage: Challenges and opportunities," *IEEE Access*, vol. 9, pp. 164223–164244, 2021.

[8] Z. Xiao et al., "LEO satellite access network (LEO-SAN) toward 6G: Challenges and approaches," *IEEE Wireless Commun.*, vol. 31, no. 2, pp. 89–96, Apr. 2024.

[9] H. K. Dureppagari, C. Saha, H. S. Dhillon, and R. M. Buehrer, "NTN-based 6G localization: Vision, role of LEOs, and open problems," *IEEE Wireless Commun.*, vol. 30, no. 6, pp. 44–51, Dec. 2023.

[10] S. Buzzi et al., "Multi-satellite diversity through the use of OTFS," in *Proc. 39th Int. Commun. Satell. Syst. Conf. (ICSSC)*, Oct. 2022, pp. 273–274.

[11] S. Buzzi et al., "LEO satellite diversity in 6G non-terrestrial networks: OFDM vs. OTFS," *IEEE Commun. Lett.*, vol. 27, no. 11, pp. 3013–3017, Nov. 2023.

[12] Z. M. Bakhsh, Y. Omid, G. Chen, F. Kayhan, Y. Ma, and R. Tafazolli, "Multi-satellite MIMO systems for direct satellite-to-device communications: A survey," *IEEE Commun. Surveys Tuts.*, vol. 27, no. 3, pp. 1536–1564, Jun. 2025.

[13] K. Humadi, G. K. Kurt, and H. Yanikomeroglu, "Distributed massive MIMO system with dynamic clustering in LEO satellite networks," in *Proc. 6th Int. Conf. Commun. Signal Process. Appl. (ICCSPA)*, Jul. 2024, pp. 1–6.

[14] C. D'Andrea, T. Foggi, A. Piemontese, A. Ugolini, S. Buzzi, and G. Colavolpe, "Coherent vs. non-coherent joint transmission in cell-free user-centric non-terrestrial wireless networks," in *Proc. IEEE 25th Int. Workshop Signal Process. Adv. Wireless Commun. (SPAWC)*, Sep. 2024, pp. 636–640.

[15] S. Buzzi, C. D'Andrea, A. Zappone, and C. D'Elia, "User-centric 5G cellular networks: Resource allocation and comparison with the cell-free massive MIMO approach," *IEEE Trans. Wireless Commun.*, vol. 19, no. 2, pp. 1250–1264, Feb. 2020.

[16] Ö. T. Demir, E. Björnson, and L. Sanguinetti, "Foundations of user-centric cell-free massive MIMO," *Found. Trends® Signal Process.*, vol. 14, nos. 3–4, pp. 162–472, 2021.

[17] H. Q. Ngo, A. Ashikhmin, H. Yang, E. G. Larsson, and T. L. Marzetta, "Cell-free massive MIMO versus small cells," *IEEE Trans. Wireless Commun.*, vol. 16, no. 3, pp. 1834–1850, Mar. 2017.

[18] H. Q. Ngo, G. Interdonato, E. G. Larsson, G. Caire, and J. G. Andrews, "Ultradense cell-free massive MIMO for 6G: Technical overview and open questions," *Proc. IEEE*, vol. 112, no. 7, pp. 805–831, Jul. 2024.

[19] L. Miretti, G. Caire, and S. Stańczak, "Robust mmWave/sub-THz multi-connectivity using minimal coordination and coarse synchronization," *IEEE Trans. Wireless Commun.*, vol. 24, no. 1, pp. 293–308, Jan. 2025.

[20] M. M. M. Freitas, S. Buzzi, and G. Interdonato, "Eliminating phase misalignments in cell-free massive MIMO via differential transmission," *IEEE Wireless Commun. Lett.*, vol. 14, no. 9, pp. 2718–2722, Sep. 2025.

[21] A. Guidotti, A. Vanelli-Coralli, and C. Amatetti, "Federated cell-free MIMO in non-terrestrial networks: Architectures and performance," *IEEE Trans. Aerosp. Electron. Syst.*, vol. 60, no. 3, pp. 3319–3347, Jun. 2024.

[22] G. Bacci, R. De Gaudenzi, M. Luise, L. Sanguinetti, and E. Sebastiani, "Formation-of-arrays antenna technology for high-throughput mobile nonterrestrial networks," *IEEE Trans. Aerosp. Electron. Syst.*, vol. 59, no. 5, pp. 4919–4935, Oct. 2023.

[23] R. De Gaudenzi, G. Bacci, M. Luise, L. Sanguinetti, and P. Angeletti, "Applicability of CF-MIMO precoding to a formation of arrays (FoA) for mobile satellite communications," *IEEE Trans. Aerosp. Electron. Syst.*, vol. 61, no. 5, pp. 11069–11087, Oct. 2025.

[24] F. Riera-Palou, G. Femenias, M. Caus, M. Shaat, and A. I. Pérez-Neira, "Scalable cell-free massive MIMO networks with LEO satellite support," *IEEE Access*, vol. 10, pp. 37557–37571, 2022.

[25] C. Liu, W. Feng, Y. Chen, C.-X. Wang, and N. Ge, "Cell-free satellite-UAV networks for 6G wide-area Internet of Things," *IEEE J. Sel. Areas Commun.*, vol. 39, no. 4, pp. 1116–1131, Apr. 2021.

[26] T. Van Chien, A. H. Le, H. Q. Ngo, and S. Chatzinotas, "Uplink sum throughput analysis and maximization for integrated satellite-terrestrial cell-free massive MIMO," in *Proc. IEEE Global Commun. Conf.*, Dec. 2023, pp. 1435–1440.

[27] Z. Zhang, Y. Wu, Z. Ma, X. Lei, L. Lei, and Z. Wei, "Coordinated multi-satellite transmission for OTFS-based 6G LEO satellite communication systems," *IEEE J. Sel. Areas Commun.*, vol. 43, no. 1, pp. 156–170, Jan. 2025.

[28] B. De Filippo, R. Campana, A. Guidotti, C. Amatetti, and A. Vanelli-Coralli, "Cell-free MIMO in 6G NTN with AI-predicted CSI," in *Proc. IEEE 25th Int. Workshop Signal Process. Adv. Wireless Commun. (SPAWC)*, Sep. 2024, pp. 631–635.

[29] S. Kim, J. Wu, B. Shim, and M. Z. Win, "Cell-free massive non-terrestrial networks," *IEEE J. Sel. Areas Commun.*, vol. 43, no. 1, pp. 201–217, Jan. 2025.

[30] T.-N. Tran and G. Interdonato, "Energy efficiency optimization in integrated satellite-terrestrial UAV-enabled cell-free massive MIMO," in *Proc. IEEE 25th Int. Workshop Signal Process. Adv. Wireless Commun. (SPAWC)*, Sep. 2024, pp. 711–715.

[31] L. Gaudio, G. Colavolpe, and G. Caire, "OTFS vs. OFDM in the presence of sparsity: A fair comparison," *IEEE Trans. Wireless Commun.*, vol. 21, no. 6, pp. 4410–4423, Jun. 2022.

[32] E. Conti, A. Piemontese, T. Foggi, G. Colavolpe, and A. Vannucci, "Efficient message-passing detection for multi-satellite systems using OTFS modulation," in *Proc. IEEE Aerosp. Conf.*, 2025, pp. 1–11.

[33] E. Conti, A. Piemontese, T. Foggi, G. Colavolpe, and A. Vannucci, "Detection techniques for OTFS transmissions over doubly-selective channels," *IEEE Trans. Commun.*, submitted for publication.

[34] M. M. M. Freitas, S. Buzzi, and G. Interdonato, "UAV-empowered aerial cell-free networks robust to downlink phase misalignments," in *Proc. IEEE 26th Int. Workshop Signal Process. Artif. Intell. Wireless Commun. (SPAWC)*, Jul. 2025, pp. 1–5.
[35] V. Singh et al., "Diversity combining scheme for time-varying STBC NGSO multi-satellite systems," *IEEE Wireless Commun. Lett.*, vol. 28, no. 4, pp. 882–886, Apr. 2024.
[36] Q. Li, M. El-Hajjar, K. Cao, C. Xu, H. Haas, and L. Hanzo, "Holographic metasurface-based beamforming for multi-altitude LEO satellite networks," *IEEE Trans. Wireless Commun.*, vol. 24, no. 4, pp. 3103–3116, Apr. 2025.
[37] Q. Li, M. El-Hajjar, C. Xu, J. An, C. Yuen, and L. Hanzo, "Stacked intelligent metasurfaces for holographic MIMO-aided cell-free networks," *IEEE Trans. Commun.*, vol. 72, no. 11, pp. 7139–7151, Nov. 2024.
[38] Q. Li, M. El-Hajjar, Y. Sun, and L. Hanzo, "Performance analysis of reconfigurable holographic surfaces in the near-field scenario of cell-free networks under hardware impairments," *IEEE Trans. Wireless Commun.*, vol. 23, no. 9, pp. 11972–11984, Sep. 2024.
[39] P. Angeletti and R. De Gaudenzi, "Heuristic radio resource management for massive MIMO in satellite broadband communication networks," *IEEE Access*, vol. 9, pp. 147164–147190, 2021.
[40] S. Bhandari, T. X. Vu, and S. Chatzinotas, "User-centric flexible resource management framework for LEO satellites with fully regenerative payload," *IEEE J. Sel. Areas Commun.*, vol. 42, no. 5, pp. 1246–1261, May 2024.
[41] B. Ahmad, D. G. Riviello, B. De Filippo, A. Guidotti, and A. Vanelli-Coralli, "Location-assisted graph-based user scheduling in multi-user MIMO LEO NTN systems," *Int. J. Satell. Commun. Netw.*, Sep. 2025.
[42] "Propagation data required for the design systems in the land mobile-satellite service," ITU, Geneva, Switzerland, Rep. Rec. ITU-R P.681-11, Aug. 2019. [Online]. Available: https://www.itu.int/rec/R-REC-P.681-11-201908-I

CARMEN D'ANDREA (Member, IEEE) received the B.S., M.S., and Ph.D. degrees (summa cum laude) in telecommunications engineering from the University of Cassino and Southern Lazio, Italy, in 2013, 2015, and 2019, respectively, where she is currently a Tenure-Track Assistant Professor (RTT). In 2017, she was a visiting Ph.D. student with the Wireless Communications Research Group with the Department of Information and Communication Technologies, Universitat Pompeu Fabra, Barcelona, Spain. In Spring 2020, she spent three months as a Visiting Researcher with the Communication System Division, Department of Electrical Engineering, Linköping University, Sweden. Her research interests focus on wireless communication and signal processing, with emphasis on mmWave communications, massive MIMO systems, and the study of waveforms for beyond-5G communication systems. In June 2023, she received the "Best Paper Award" at EUCNC and 6G Summit. In 2023, she received the Italian Scientific Habilitation (ASN) as an Associate Professor. She was in the World's Top 2% Scientists 2023 and 2025 in the topic "Information and Communication Technologies - Networking and Telecommunications" listed by Elsevier, Scopus, and Standford University and in the list of "100 Brilliant and Inspiring Women in 6G" List for 2024. From 2019 to 2024, she served as an Associate Editor for IEEE OPEN JOURNAL OF THE COMMUNICATIONS SOCIETY. Since 2020, she has been an Associate Editor of IEEE COMMUNICATIONS LETTERS (Exemplary Editor in 2022 and 2024) and in 2025, she started serving as an Associate Editor for IEEE TRANSACTIONS ON WIRELESS COMMUNICATIONS. She serves regularly as a TPC member for several international conferences.

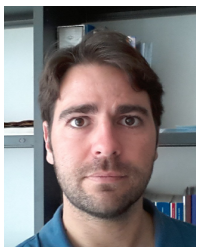

TOMMASO FOGGI (Member, IEEE) received the master's degree in telecommunication engineering and the Ph.D. degree in information technology from the University of Parma in 2003 and 2008, respectively. From 2009 to 2018, he was a Research Engineer with the National Inter-University Consortium for Telecommunications (CNIT) in the University of Parma Research Unit. He is currently an Associate Professor with the Engineering and Architecture Department, University of Parma. He is author of tens of peer-reviewed papers and several patents. He was/is involved in many research projects funded by public authories like MIUR, ESA, EU or private companies like Ericsson, CGS, Inmarsat, Huawei. His main research interests include electronic signal processing for optical and satellite communication systems. He won the Best Paper Award in the Optical Networks and Systems Symposium at the IEEE International Conference on Communications, Beijing, China, in May 2008.

AMINA PIEMONTESE (Member, IEEE) received the Dr.Ing. degree in telecommunications engineering from the University of Parma, Italy, in 2006, and the Ph.D. degree in information technology from the University of Parma and from TELECOM Bretagne, Brest, France, in 2011. From 2011 to 2015, she held a postdoctorate position with the Department of Engineering and Architecture, University of Parma, where she is currently an Associate Professor. From May 2015 to May 2020, she was with the Department of Electrical Engineering, Chalmers University of Technology, Gothenburg, Sweden. Her research activity includes various topics in digital communications, with particular emphasis on iterative joint detection and decoding algorithms, multiuser communications theory, and information theory. She received the Best Paper Award at the 5th Advanced Satellite Mobile Systems Conference and 11th International Workshop on Signal Processing for Space Communications in 2010 and at the IEEE Wireless Communications and Networking Conference, and the Marie Curie Individual Fellowship of the European Commission.

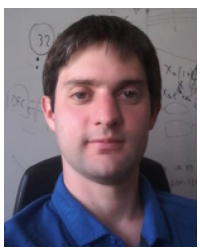

ALESSANDRO UGOLINI (Member, IEEE) received the master's degree (cum laude) in telecommunications engineering and the Ph.D. degree in information technology from the University of Parma in 2012 and 2016, respectively. In 2012, he received a National Inter-University Consortium for Telecommunications (CNIT) Grant and a Research Grant funded by the Department of Information Engineering (DII), University of Parma, for the study of synchronization algorithms for spectrally efficient systems. In 2016, he was a Postdoctoral Researcher with DII. In 2017, he was a Visiting Researcher with the Communication and Antenna Systems Division, Chalmers University of Technology, Gothenburg, Sweden, and also with the Interdisciplinary Centre for Security, Reliability and Trust, University of Luxembourg. From 2017 to 2025, he was an Assistant Professor with the Department of Engineering and Architecture, University of Parma, where he is currently an Associate Professor. His main research interests include digital, wireless, and satellite communications, applied information theory, detection and synchronization schemes. He received the Best Paper Award at the IEEE Wireless Communications and Networking Conference in 2019.

STEFANO BUZZI (Senior Member, IEEE) received the M.Sc. degree (summa cum laude) in electronic engineering and the Ph.D. degree in electrical and computer engineering from the University of Naples Federico II in 1994 and 1999, respectively. He had short-term research appointments with Princeton University, Princeton, NJ, USA, in 1999, 2000, 2001, and 2006. He joined the University of Cassino and Southern Lazio, Italy, in 2000, where he was an Assistant Professor and has been an Associate Professor since 2002 and a Full Professor since 2018. He was the General Coordinator of the EU-Funded Innovative Training Network Project METAWIRELESS, on the application of metasurfaces to wireless communications, and currently the General Coordinator the EU-Funded Doctoral Network ISLANDS, on integrated sensing and communications for the vehicular environment. He has coauthored about 180 technical peer-reviewed journals and conference papers, and, among these, the highly cited paper "What will 5G be?," IEEE JOURNAL ON SELECTED AREAS IN COMMUNICATIONS in June 2014. His current research interests include communications and signal processing, with an emphasis on wireless communications and beyond-5G systems. He is a former Associate Editor of IEEE SIGNAL PROCESSING LETTERS and IEEE COMMUNICATIONS LETTERS, and has been the Guest Editor of four IEEE JOURNAL ON SELECTED AREAS IN COMMUNICATIONS special issues. From 2014 to 2020, he was an Editor of IEEE TRANSACTIONS ON WIRELESS COMMUNICATIONS. He is currently an Associate Editor of IEEE TRANSACTIONS ON COMMUNICATIONS. He serves regularly as a TPC member for several international conferences.

GIULIO COLAVOLPE (Senior Member, IEEE) received the Dr.Ing. degree (cum laude) in telecommunications engineering from the University of Pisa, Italy, in 1994, and the Ph.D. degree in information technologies from the University of Parma, Italy, in 1998. Since 1997, he has been with the University of Parma, where he is currently a Professor of Telecommunications with the Dipartimento di Ingegneria e Architettura. In 2000, he was Visiting Scientist with the Institut Eurécom, Valbonne, France. In 2013, he was a Visiting Scientist with the European Space Agency (ESTEC) Noordwijk, The Netherlands. His research activity has led to more than 200 papers in refereed journals and in leading international conferences, and 18 industrial patents. His research interests include the design of digital communication systems, adaptive signal processing (with particular emphasis on iterative detection techniques for channels with memory), channel coding, and information theory. He received the Best Paper Award at the 13th International Conference on Software, Telecommunications and Computer Networks, Split, Croatia, September 2005, the Best Paper Award for Optical Networks and Systems at the IEEE International Conference on Communications, Beijing, China, May 2008, and the Best Paper Award at the 5th Advanced Satellite Mobile Systems Conference and 11th International Workshop on Signal Processing for Space Communications, Cagliari, Italy. He served as an Editor for IEEE TRANSACTIONS ON WIRELESS COMMUNICATIONS, IEEE TRANSACTIONS ON COMMUNICATIONS, and IEEE WIRELESS COMMUNICATIONS LETTERS, and as an Executive Editor for *Transactions on Emerging Telecommunications Technologies*.